Journal of Materials Chemistry A

ROYAL SOCIETY OF CHEMISTRY

REVIEW

View Article Online
View Journal | View Issue

Cite this: *J. Mater. Chem. A*, 2026, **14**, 20637

Stimuli-responsive material-based smart supercapacitors: design, progress, and perspectives

Wenwen Liu, *[a] Hongling Li, [a] Elena Bekyarova, [b] Roland Yingjie Tay *[a] and Aiping Yu *[c]

With the rapid development of portable/wearable electronics, it is highly desirable to develop external stimuli-responsive (*e.g.*, temperature, magnetic field, light, and voltage) energy storage systems to meet the requirements of these devices. Among them, stimulus-responsive material-based smart supercapacitors (SCs) have attracted much attention due to their combination of SC advantages and specific responses to environmental stimuli. As a key component of such smart devices, stimuli-responsive materials play a significant role in the design of smart SCs. Despite some progress, the design, fabrication, and application of multi-responsive materials for building smart SCs are still in the early stages, especially regarding the effects of each force/stimulus on capacitive behavior. Therefore, it is vital to summarize the research studies and developments, which are not only instructive for researchers in this field but also crucial for the development of other smart energy storage devices. In this scenario, our review timely summarizes the latest reported stimuli-responsive material-based SCs, covering their fundamental principles, design strategies, and configurations as well as their capacitive behaviour correlated to external forces/stimuli. Particularly, the different ways in which external forces/stimuli can interact with the components of SCs are discussed. Furthermore, future perspectives and challenges in this field for the development of multi-responsive electrode-material-based smart SCs are highlighted. Additionally, it is expected that this summary will place stimulus-responsive SCs in practical applications and provide insights for the design of other smart energy storage devices.

Received 23rd January 2026
Accepted 14th April 2026

DOI: 10.1039/d6ta00650g

rsc.li/materials-a

[a]*School of Electrical and Electronic Engineering, Nanyang Technological University, 50 Nanyang Avenue, Singapore 639798, Singapore. E-mail: wenwen.liu@ntu.edu.sg; rolandtay@ntu.edu.sg*

[b]*University of California-Riverside, 900 University Ave, Riverside, CA 92521, USA*

[c]*Department of Chemical Engineering, Waterloo Institute for Nanotechnology, University of Waterloo, Waterloo N2L 3G1, Canada. E-mail: aipingyu@uwaterloo.ca*

Wenwen Liu

*Wenwen Liu is currently a Senior Research Scientist at Nanyang Technological University. He received his PhD degree in Chemical Engineering in 2020 from the University of Waterloo. Before joining Nanyang Technological University, he was a Research Scientist at the A*STAR Institute of Materials and Research Engineering from 2020 to 2023. His research involves the synthesis and engineering of nanomaterials and their applications in energy storage and conversion systems, such as supercapacitors, lithium-ion batteries, metal–air batteries, and water splitting.*

Hongling Li

Hongling Li is currently a Senior Research Fellow in the School of Electrical and Electronic Engineering at Nanyang Technological University. She received her PhD degree from the College of Chemistry and Chemical Engineering, Lanzhou University, in 2012. Her current research interests focus on advanced low-dimensional materials such as graphene and boron nitride and their applications in energy storage and thermal management.

1. Introduction

Currently, with the rapid development of novel wearable electronics and sensors, energy storage devices are required to possess characteristics such as lightweight design, mechanical flexibility, miniaturization, and environmental adaptability. However, traditional energy storage devices cannot fully satisfy these requirements.[1,2] Therefore, it is necessary to explore appropriate energy storage systems to meet these new demands. Among them, stimuli-responsive material-based smart supercapacitors (SCs) have received increasing attention.[3,4] They not only inherit the advantages of SCs (*e.g.*, excellent power density and long cycle life) but also exhibit multi-functionality towards environment stimuli.[5,6] As reported, the overall performance of SCs mainly depends on the electrode materials and/or electrolytes, so stimuli-responsive materials with the characteristics of interaction and/or self-regulation towards external stimuli play a significant role in the construction of smart SCs.[7–9] Therefore, researchers have made efforts to explore suitable stimuli-responsive materials and to design stimuli-responsive smart SCs.[10–14] Although the research in this related field is still in the early stages, progress has been made in recent years, and this area of research has become a hot topic.[8,15] More importantly, it is predicted that there will be a flourishing growth of the stimuli-responsive material-based smart SCs in the next few years. Hence, it is necessary to summarize these research findings, progress, and breakthroughs, thereby providing useful guidance for this emerging field. However, systematic summaries of the specific applications of stimuli-responsive materials in smart SCs remain limited, despite their importance in guiding research in this field. Therefore, a comprehensive review is highly desired to summarize the recent progress in the design and construction of stimuli responsive smart SCs, with particular emphasis on the specific effects of external forces/stimuli on the electrochemical performance.

Bearing this in mind, our review paper timely fills the gap and primarily covers the design of external stimuli-responsive materials/electrolytes, as well as the appropriate application of these forces/stimuli to design stimuli-responsive SCs. First, the background and motivation for the development of external-stimuli-responsive smart SCs are briefly introduced. Then, the principles of stimuli-responsive materials and their responsive properties are presented. Next, the latest progress in stimuli-responsive material-based smart SCs in response to various external stimuli (*e.g.*, temperature, magnetic field, light, and voltage) is systematically summarized. This paper delves into the specific effects of external forces/stimuli on the electrochemical performance of SCs, particularly the different ways in which external forces/stimuli interact with the various components. Furthermore, future perspectives and challenges in the construction of stimuli-responsive material-based smart SCs are discussed. This review not only provides insights into the

Elena Bekyarova

Elena Bekyarova is an Associate Research Professor at the University of California, Riverside. Her research lies at the intersection of materials science and nanotechnology, with expertise in carbon nanomaterials, thin films, and functional nanostructures. Her work spans adsorption, synthesis, and materials chemistry, with applications in energy storage, electronics, sensing technologies, and biomedicine. She is currently focused on developing novel carbon nanomaterials for energy applications, electronics, and biomedical devices.

Roland Yingjie Tay

Roland Yingjie Tay is an Assistant Professor in the School of Electrical and Electronic Engineering (EEE) at Nanyang Technological University (NTU). He received his B. Eng and PhD degree in EEE from NTU in 2009 and 2016, respectively. In 2021, he was awarded the International Postdoctoral Fellowship (IPF) at NTU and completed his postdoctoral fellowship at the California Institute of Technology (Caltech). His research focuses on the synthesis and development of low-dimensional nanomaterials, and their employment in various applications including thermal management, electromagnetic interference shielding, flexible electronics, energy and sensor devices, and materials for harsh environments.

Aiping Yu

Aiping Yu is a University Research Chair professor in the Department of Chemical Engineering at the University of Waterloo, a Fellow of the Canadian Academy of Engineering, Director of the Carbon Nanomaterials Laboratory at the University of Waterloo, and an Associate Editor of Chemical Engineering Journal and Carbon Energy. She possesses multidisciplinary expertise in the development, processing, and chemical functionalization of nanomaterials and their applications in energy storage and multifunctional polymer composites. She has achieved 9 US patents/provisional patents and published 3 books/book chapters, and over 260 papers in peer-reviewed journals.

development of such smart SCs but also offers useful guidance for the design of other smart energy storage devices and inspires innovative concepts for future research.

2. Design of stimuli-responsive electrode/electrolyte materials

Stimuli-responsive materials that change their properties or states in response to external stimuli (*e.g.*, temperature, magnetic field, light, and voltage), are also denoted as "smart materials"[16,17] and are highly desirable in various applications, such as memory devices, artificial muscles, and energy storage systems (Fig. 1).[18,19] This inherent responsiveness allows for the development of adaptive and controllable electrochemical devices like sensors, actuators, and SCs.[20–25] Among them, the stimuli-responsive behavior of SCs stems from the fundamental interaction between the designed electrode/electrolyte and external forces/stimuli (Table 1). Stimuli-responsive materials are key components of smart responsive SCs, which has spurred the development of various strategies to design and synthesize different materials/components with unique responsive properties.[26–30] To better understand the internal logic of the design of smart SCs based on these stimuli-responsive materials, we briefly introduce the working principle of these materials interacting with the external stimuli such as temperature, magnetic field, light, and voltage, and outline the effects of these external stimuli on their capacitive behavior.

2.1 Temperature-responsive material-based SCs

Most thermoresponsive materials are smart polymers whose functional properties (*e.g.*, hydrophilic–hydrophobic properties and electrical conductivity) change significantly when the temperature exceeds a certain threshold, known as the critical solution temperature.[31–33] These changes effectively suppress ion or electron conduction between electrodes. Generally, the thermo-responsive behavior can be classified into two types:

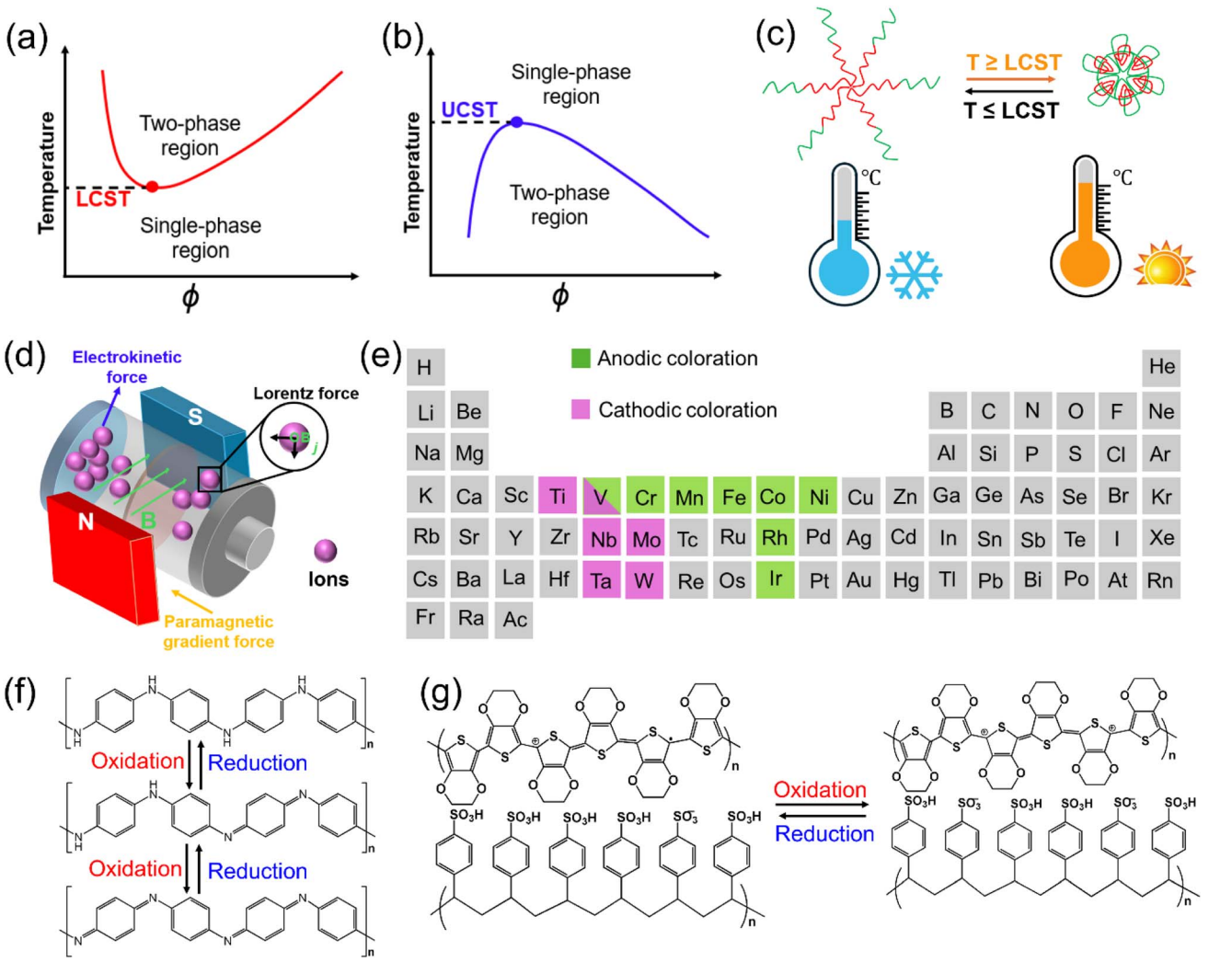

Fig. 1 Phase diagram for polymer/solvent mixtures with different thermo-responsive behaviors: (a) LCST and (b) UCST. (c) Illustration of the structural change of the polymer electrolyte with LCST during the heating/cooling cycle. (d) Illustration of the main body forces generated on SCs in a magnetic field. (e) Anodic coloration and cathodic coloration related to transition metal oxides. Electrochromic mechanism of (f) PANI and (g) PSS-PEDOT.

Table 1 Comparison of advantages and disadvantages of different external force/stimuli-based smart SCs

Stimulus type	Mechanism	Key advantages	Key disadvantages/challenges
Temperature	Material functional properties (*e.g.*, hydrophilic–hydrophobic properties, electrical conductivity) change significantly when the temperature exceeds a certain threshold	Reversibly switching off capacitance when overheating and automatically restoring function upon cooling; absorbing/releasing heat during phase transitions and stabilizing internal temperature and performance in both low and high conditions; improving energy density through voltage extension; exhibiting good mechanical stability under deformation	Complex material engineering to create stable dual-zone phase-change materials; slower physical phase transitions causing slow response time; non-conductive phase change materials or thermally-gating polymers reducing the electrode's conductivity or overall specific capacitance
Magnetic field	The co-existence of electric current and changes in electric field are usually accompanied by the generation of a magnetic field	Manipulating ions without physical connections; accelerating ion transport at the electrode interface for fast charging/discharging; aligning electrodes for better performance during fabrication	Early research stage with limited real applications; incorporating magnetic materials, resulting in complexity and high cost; unclear fundamental mechanisms
Light	When light hits a photoactive electrode, it excites electrons, creating electron–hole pairs. These charges are then separated, in which electrons are stored at the electrode interface and holes participate in reactions, thus boosting charge storage capability	Reducing external charging and creating a self-powered device; enabling novel features to be integrated into displays and other devices	Integrating light-harvesting and storage modules, thus leading to lower photovoltaic conversion efficiency and internal resistance; complex design process for effective photoactive electrodes with suitable band gaps, efficient charge separation, and long-term stability; easily recombining photogenerated charge carriers before being stored
Voltage	It is a fascinating synergy where energy storage and color changes happen simultaneously, leveraging a single electrochemical reaction to perform both capacitor and electrochromic functions	Ability to visually indicate energy storage levels in real time; combining energy storage modulation and optical modulation, which is ideal for smart windows and displays	Material compromise because electrode materials must excel at both energy storage and electrochromic performance; slow response time limiting practical application; repeated color switching and charge/discharge cycles cause material degradation, delamination and performance fading; difficulty in balancing optical contrast, coloring efficiency, energy density, and cycle life

lower critical solution temperature (LCST) (Fig. 1a) and upper critical solution temperature (UCST) (Fig. 1b)[34–36]. LCST refers to the temperature above which the polymer separates and becomes turbid due to its reduced solubility, while the solution becomes clear and transparent again below the LCST. Regarding UCST, it refers to the temperature at which the polymer becomes insoluble, and phase separation occurs. Here, LCST thermo-responsive polymers (*e.g.*, poly(*N*-isopropylacrylamide) (PNIPAM) and its derivatives) are used as examples to illustrate their working principles (Fig. 1c). Below the LCST, the polymers absorb water, swell, and become hydrophilic. Conversely, above the LCST, hydrophobic interactions dominate, forcing water to escape, causing the polymer to collapse and become hydrophobic. The reversible temperature-triggered behavior leads to significant changes in ion transport and/or conductivity, making them ideal materials for designing thermoresponsive SCs.

Recently, thermoresponsive polymers (*e.g.*, PNIPAM[37–39]) and their copolymers (NIPAM copolymerized with acrylic acid (AA),[11,40] acrylamide (AM)[26,41] and methylcellulose (MC)[42,43]) have been employed to design the thermoresponsive smart SCs and other energy storage devices. As reported, thermoresponsive smart SCs can be achieved by integrating thermoresponsive polymers into SC components (*e.g.*, electrode materials and electrolytes) based on different functional mechanisms.[44] From a material perspective, a common strategy for designing thermoresponsive smart SCs is to integrate thermoresponsive materials into electrodes.[45] These thermoresponsive electrodes consist of conductive fillers and a specific polymer with a large coefficient of thermal expansion. When increasing temperature, the volume expansion of the polymer increases the distance between conductive fillers, which results in a decrease of few orders of magnitude in the conductivity of the thermoresponsive electrode. There is no doubt that the fast and reversible thermoresponsive electrodes with self-adjustable conductivity enable the conductive filler/polymer composites to be promising materials for the design of thermoresponsive smart SCs. Moreover, the modification of electrode materials with

thermoresponsive polymers is also employed to construct smart thermoresponsive SCs.[27] In this scenario, the thermoresponsive polymer acts as a valve to promote and prevent the diffusion of electrolyte ions through its configuration changes under cooling/heating conditions. This general and promising approach can be extended to functionalize other components of SCs, thus enabling the obtained smart SCs with thermal responsibility. Apart from the design of thermoresponsive electrodes, another strategy is to explore thermoresponsive electrolytes to control ion diffusion under different temperature conditions.[11,26] The thermoresponsive electrolytes with reversible sol–gel transition phases have attracted widespread attention. The sol–gel transition process is determined by the LCST, which has a significant impact on the electrolyte ion diffusion rate. When the temperature is above the LCST, the polymer molecular chains form micelles, which generate a gel network due to hydrophobic interactions, thus suppressing the free migration of ions. When the temperature is below LCST, the strong hydrogen bonding between the polymers and the solvent molecules leads to polymer dissolution, thereby facilitating the migration of ions.[22,44]

2.2 Magnetic field-responsive material-based SCs

Clearly, magnetic fields affect electrochemical processes, but the underlying mechanism of these effects is a cross-disciplinary concept involving physics, chemistry, materials science, electrochemistry, and magnetism. In this case, a better understanding of the effect of an external magnetic field on the electrochemical behavior of SC devices could lead to significant breakthroughs in the design of high-performance magnetic field-responsive SCs. From a physics point of view, according to Faraday's law of electromagnetic induction, the co-existence of electric current and changes in the electric field is usually accompanied by the generation of a magnetic field.[46–49] Generally, the main driving forces for the movement of electrolyte ions during charge/discharge processes are electromigration, diffusion, and convection. However, when a magnetic field is applied, five additional body forces are introduced (Fig. 1d),[48] which include the paramagnetic gradient force (F_p), field gradient force (F_B), Lorentz force (F_L), electrokinetic force (F_E) and magnetic damping force (F_M). The definitions and calculations of these five body forces are briefly described as follows:

(a) Paramagnetic gradient force (F_p) is generated by the interaction between an applied magnetic field and the concentration gradient of paramagnetic species. It can be calculated using eqn (1):

$$\overrightarrow{F_p} = \frac{x_m B^2 \overrightarrow{\nabla} c}{2\mu_0} \quad (1)$$

where x_m, B, ∇, c, and μ_0 refer to the molar susceptibility, the magnetic field strength, the del operator, the concentration and the permeability of free space,[50,51] respectively.

(b) Field gradient force (F_B) is a force that arises when a magnetic substance is placed in a non-uniform magnetic field. It is expressed as eqn (2):

$$\overrightarrow{F_B} = \frac{x_m c B \overrightarrow{\nabla B}}{2\mu_0} \quad (2)$$

where x_m, B, ∇B, c, and μ_0 refer to the molar susceptibility, the magnetic field strength, the magnetic gradient, the concentration and the permeability of free space,[52,53] respectively.

(c) Lorentz force (F_L) is the total electromagnetic force acting on a charged particle moving with velocity through electric and magnetic fields.[54] The Lorentz force is given by eqn (3):

$$F_L = q(E + v_d \times B) \quad (3)$$

where E, v_d, q and B are the electric field, the drift velocity, the charge, and the magnetic field strength, respectively.

(d) Electrokinetic force (F_E) refers to forces generated at the interface of a charged surface and a liquid, causing motion of particles or fluid due to electric fields.[54] The electrokinetic force (F_E) can be described using eqn (4):

$$\overrightarrow{F_E} = \sigma_d \overrightarrow{E_{\parallel}} \quad (4)$$

where σ_d is the total charge density in the diffuse layer, and $E_{\parallel}$ is the effective electric field.

(e) Magnetic damping force (F_M) is a non-contact force that slows or stops the motion of a conductor by converting its kinetic energy into heat, generated by eddy currents induced when the conductor moves through a magnetic field. The magnetic damping force is given by eqn (5):

$$\overrightarrow{F_M} = \sigma \overrightarrow{v} \times \vec{B} \times \vec{B} \quad (5)$$

where σ, v, and B are the conductivity of the conductor, the velocity of the magnet/conductor, and the magnetic field strength, respectively.[51,54]

Based on the working principle of SCs, their energy storage mechanism relies on the adsorption/desorption of electrolyte ions at the electrode/electrolyte interface or involves surface redox reactions during the charge/discharge process. Nonetheless, compared with the fast electron transfer, the slow mass transport limits the performance (*e.g.*, operating voltage and power density) of SCs. From this point of view, mass transport is considered one of the key processes,[55] typically controlled by diffusion and migration, while the contribution of convection is negligible.[56] In this case, an applied magnetic field provides an effective method to accelerate mass transport. In short, when a magnetic field interacts with the ionic current in the electrolyte, convection is generated, thereby increasing the diffusional mass transfer rate and resulting in a narrower diffusion layer. The Lorentz force is reported to be the dominant magnetic force causing this effect.[55] Furthermore, when the field gradient force is comparable in magnitude to the Lorentz force, it is believed to have a similar effect on mass transport.[50–52,57] In this case, when a magnetic field is applied to an electrochemical cell, a convection effect through ion movement occurs due to the magnetohydrodynamic effect, thereby resulting in a decrease in the thickness of the diffusion layer and the enhancement of mass transport.[54] Additionally, a study reveals that the effect of the magnetic field on the performance of SCs is strongly dependent on the concentration and types of electrolytes used.[46]

According to the above discussion and analysis, a magnetic field can affect the electrochemical process in the following ways: (1) modifying the properties of electrodes and/or electrolytes through the variation of the Hall effect and electrical conductivity; (2) controlling the mass transport *via* the superposition of the magnetic fields generated by the interaction of magnetohydrodynamic phenomena near the electrodes and the convective diffusion layer; (3) varying the electrochemical kinetics during the electrochemical process. In short, the magnetic field can influence the kinetics of electrolyte ions, electrode/electrolyte interactions, and the morphology and quality of the final product, thus providing a promising opportunity to design magnetic field-responsive SCs.[54]

2.3 Light-responsive material-based SCs

Light-responsive SCs are usually described as having capacitive behavior that responds to light or can be tailored by harnessing light energy. Therefore, light-driven SCs have opened new possibilities for smart energy storage applications. Light-driven SCs include three-electrode photo-driven SCs and two-electrode photo-driven SCs[58,59]. Generally, a three-electrode photo-driven SC has a dual-function intermediate electrode between the photoelectrode and the counter electrode, dividing the device into two sections: one for photoelectric conversion and the other for energy storage. For two-electrode photo-driven SCs, the design strategy is to integrate the energy generation and storage modules into a single device, thereby significantly simplifying the design and construction of photo-assisted charging SCs. Additionally, compared to three-electrode photo-driven SCs, the two-electrode system is a novel and compact system with advantages such as ease of assembly, low cost, and good cycling stability. Therefore, the photo-driven SCs presented in this review focus on two-electrode photo-SCs unless otherwise mentioned.[60]

Light-responsive material-based SCs utilize photo-generated holes/electrons on the surface of the photoelectrode to participate in energy storage. Concisely, when the photoactive materials are exposed to light, they generate electron–hole pairs. The rapid separation and transfer of these photogenerated charges enable them to enhance the electric double-layer formation or participate in reversible faradaic redox reactions. Therefore, light irradiation can boost capacitance by increasing carrier density, promoting interfacial polarization, or driving charge transfer in engineered heterojunctions. In this system, light is applied to drive the photo-responsive materials by providing adjustable radiation energy. To interact with light irradiation, the photo-responsive materials for light-driven SCs should possess both photosensitive and pseudocapacitive properties. The ideal electrode materials should meet the following requirements: (1) an appropriate band gap to absorb more light; (2) a high separation efficiency of photo-generated electrons and holes. Among them, semiconducting materials seem to be the preferred options for designing the photo-driven SCs.

2.4 Potential responsive material-based SCs

Currently, the design of smart SCs with electrochromic properties and good capacitive behavior has attracted tremendous interest. Generally, the electrochromic behavior results from the redox reactions between the electrode material and the inserted ions under an applied voltage.[61,62] It is worth noting that pseudocapacitors also rely on the reversible redox reaction of materials. Therefore, combining electrochromism and energy storage capability to manufacture electrochromic energy storage devices is an excellent choice for designing voltage-responsive smart SCs. Electrochromic materials, as important components of electrochromic smart SCs, can be divided into three types: inorganic materials, organic materials, and hybrid materials. Owing to their different coloration mechanisms, these three types of electrochromic materials display different electrochromic properties in terms of response speed, color variation, and stability.

2.4.1 Mechanism of inorganic materials. Among these inorganic oxides, metal oxides are the most used electrochromic materials, such as WO_3, V_2O_5, MoO_3, Nb_2O_5, NiO, and MnO_2.[63,64] It is noted that different electrochromic materials exhibit quite diverse color-change potential ranges, based on which the electrochromic materials can be split into two types: anodic and cathodic electrochromic materials (Fig. 1e). Generally, the cathodic metal oxide materials are colored due to the insertion of electrolyte ions during the reduction process, while the anodic metal oxide materials were colored because of the extraction of corresponding ions during the oxidation process. The cathodic metal oxide materials, such as MoO_3 and WO_3, possess unpaired single electrons in the d orbital, which is beneficial for cathodic charge injection, thus leading to reversible changes in the valence state and inducing the reversible color change. Here, WO_3, a widely studied transition-metal oxide, is used as an example to reveal the color-change mechanism of cathodic electrochromic materials. The coloration and bleaching processes of WO_3 are attributed to the insertion/extraction of cations, which can be explained as follows:

$$WO_3\ (\text{colorless}) + xM^+ + xe^- \leftrightarrow M_xWO_3\ (\text{blue}) \quad (6)$$

where M^+ refers to the cations (*e.g.*, H^+ and Li^+), and the x value is between 0 and 1. Moreover, the electrochromic properties (*e.g.*, coloration efficiency, switch speed, and stability) of WO_3 are also associated with the crystallinity.[20,65]

On the other hand, anodic coloring effects can be seen in NiO, MnO_2, and Co_3O_4. These metal oxides are typically used as counter electrodes, combined with cathodic electrochromic electrodes to form devices. As a representative anodic coloration material, the reversible color change mechanism of NiO_x is shown as follows:

$$NiO_x + \alpha Li^+ + \alpha e^- \rightarrow Li_\alpha NiO_x \quad (7)$$

$$Li_\alpha NiO_x\ (\text{bleached}) \leftrightarrow \gamma Li^+ + \gamma e^- + Li_\beta NiO_x\ (\text{colored}) \quad (8)$$

where $\alpha = \beta + \gamma$. Obviously, the color change of NiO_x is due to the intercalation/deintercalation of Li^+, which causes a change in the valence state. Additionally, it is interesting to note that vanadium oxides can be used as both cathodic electrochromic

materials and anodic electrochromic materials. Such bifunctional electrochromic properties enable their multicolor change properties.[66] Besides, apart from the above-mentioned metal oxides, metal complexes, such as Prussian blue, metal phthalocyanine, and their derivatives, are another type of inorganic electrochromic materials, which exhibit multicolor switching properties. The color change of the metal complexes is related to the redox reaction of the center metal ion as well as the involved ligands.[67–69]

2.4.2 Mechanism of organic materials. Apart from inorganic materials, organic materials, such as organic molecules, conjugated polymers, and metal organic chelates, also show electrochromic characteristics by offering multiple colors under different applied biases. Among these organic materials, small molecules such as viologens and anthraquinones are widely used as electrochromic materials due to their multi-color properties under different potentials.[70] Particularly, viologens (1,1′-disubstituted-4,4′-dipyridinium salts), a well-studied species with three reversible redox states, exhibit good electrochromic properties.[71] Furthermore, the nitrogen substituents (–*R*1 and –*R*2) in their molecule structure can be modified, thus enabling the resulting viologens to display diverse colors.[21]

In addition, conjugated polymers, which are another broad class of polymers with alternating single/double bonds, such as polyaniline (PANI), poly(3,4-ethylenedioxythiophene)–poly(-styrene sulfonic acid) (PEDOT:PSS), offer fast switching, high efficiency, and varied colors. Depending on the applied potential and the doping states, conjugated polymers can show different colors.[63] As a typical conjugated polymer, PANI exhibits reversible multicolor change due to the anion injection/extraction process (Fig. 1f).[72] PEDOT:PSS, as another typical cathodic electrochromic material, has also attracted great interest, and its corresponding electrochromic mechanism is shown in Fig. 1g. During the negative scan, the doping of electrolyte ions into the polymer backbone causes the color to change from light blue to dark blue,[73,74] while the color returns to light blue because of the de-doping process on the reverse scan, thus achieving electrochromic properties.

3. Various stimuli-responsive SCs

SCs can be engineered to respond to external stimuli (*e.g.*, temperature, magnetic fields, light, and voltage), thus achieving intelligent functionality.[75,76] For example, photostimuli-responsive SCs can reversibly change their capacitance by adjusting charge transfer at the interface under light, thus functioning as light-controlled switches for energy storage. These stimuli-responsive "smart" SCs can change their electrical or physical properties in real time, going beyond simple energy storage devices. Typically, the design of stimuli-responsive SCs involves the interdisciplinary integration of multiple disciplines. The related common processes for the construction of smart SCs can be summarized as follows: (1) determining the external stimulus required for SCs based on the specific application; (2) selecting appropriate stimuli-responsive materials; (3) organically integrating the stimuli-responsive materials into the electrode structure design; (4) characterizing and evaluating the performance of the stimuli-response electrodes/electrolytes and the fabricated SCs. This section mainly focuses on the representative examples for the design and preparation of various stimuli-responsive materials using different methods and precursors, and their applications in constructing SCs that respond to specific external stimuli such as temperature, magnetic field, light, and voltage.

3.1 Temperature-responsive SCs

Stimuli-responsive polymers usually alter their properties (*e.g.*, solubility, ion transport, and conductivity) when the external temperature exceeds a certain threshold, known as the critical solution temperature. The reversible temperature-triggered behavior leads to significant changes in their physicochemical properties, making them ideal materials for designing thermoresponsive SC applications. From an application perspective, dual thermally responsive polymers exhibiting LCST or UCST behavior are attractive because they possess the potential to be designed into smart materials that respond within a range of specific environmental variables.[35] In this case, these polymers show LCST or UCST behavior, which makes them suitable for the design of thermoresponsive smart components, thus enabling the construction of thermoresponsive smart SCs. Currently, these thermoresponsive polymers can be divided into three categories: (i) PNIPAM-based polymers, (ii) poly(ethylene oxide) (PEO)/poly(propylene oxide) (PPO)-based polymers, and (iii) cellulose derivatives[34,77].

3.1.1 PNIPAM-based polymers for temperature-responsive SCs. By integrating thermally responsive polymers in SC components (*e.g.*, electrodes, electrolytes, and separators), self-adjustment smart SCs can be achieved based on different functional mechanisms. PNIPAM is a water-soluble polymer known for its thermoresponsive nature. Briefly, it exhibits hydrophilic properties when the temperature is below LCST (32 °C), while it becomes hydrophobic and insoluble when the temperature is above LCST.[36] The temperature-dependent properties make it a promising candidate for the development of smart SCs. However, the relatively low LCST limits the operating temperature range of SCs and practical applications. In this case, it is necessary to explore a new system for performance improvement. As a pioneering research work, a reversible thermally responsive polymer based on PNIPAM and AA copolymers was designed as an electrolyte,[11] where PNIPAM governs the thermal properties, while AA provides the electrolyte ions. The thermal switching properties of this electrolyte are investigated (Fig. 2a). With the increase in temperature from 22 to 70 °C, the color of PNIPAM–AA copolymer solution changes from clear and transparent to milky white with precipitate, accompanied by a decrease in conductivity from about 180 to 20 μS cm^{-1}. Its corresponding electrochemical behavior under cooling and heating condition is studied from cyclic voltammetry (CV) curves (Fig. 2b and c). When the electrolyte temperature increases from 20 to 50 °C, the redox peaks of the PANI electrode disappear and the area enclosed by the CV curve greatly decreases, which are attributed to a thermal activated phase transition occurring in the PNIPAM–AA copolymer,

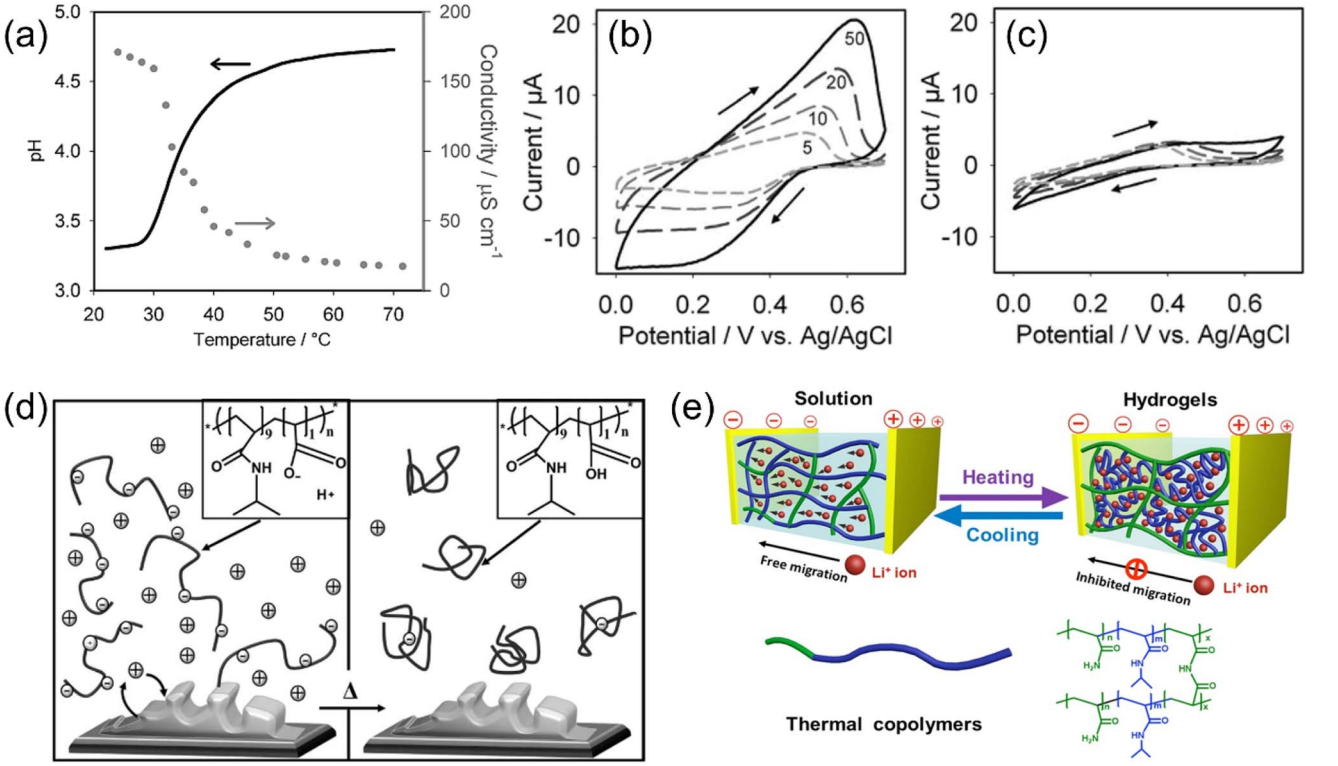

Fig. 2 (a) Ionic conductivity of the optimized PNIPAM–AA copolymer electrolyte. CV curves of PANI in the optimized PNIPAM–AA copolymer electrolyte at (b) 22 °C and (c) 50 °C, respectively. (d) Illustration of the phase change of the PNIPAM–AA copolymer at room temperature (left) and temperature above the LCST (right).[11] Reproduced with permission.[11] Copyright 2012, Wiley-VCH. (e) Illustration of sol–gel transition of LiOH–PNIPAM/AM electrolyte during the heating/cooling cycles.[26] Reproduced with permission.[26] Copyright 2015, Wiley-VCH.

resulting in decreased availability of electrolyte ions and reduced ion conductivity (Fig. 2d). In contrast, when the operating temperature decreases, the redox peaks on the CV curve appear again. This is because the polymer re-dissolves into solution and more free ions are involved in the PANI redox reaction. The recovery property suggests the reversible thermal responsiveness of the polymer electrolyte, thus enabling its used in smart SCs.

Inspired by this groundbreaking research on the PNIPAM-based electrolyte, a series of PNIPAM-based thermoresponsive copolymer electrolytes have been synthesized to construct thermoresponsive SCs. Particularly, the thermoresponsive electrolytes with a reversible sol–gel transition phase *versus* temperature have a significant impact on the electrolyte ion diffusion rate, thus leading to different electrochemical performance and making them promising candidates to build temperature responsive SCs. As a representative example, a copolymer, poly(*N*-isopropylacrylamide-*co*-acrylamide) mixed with LiOH (LiOH–PNIPAM/AM),[26] was designed. It is noted that the Li^+ diffusion coefficient in LiOH–PNIPAM/AM electrolyte significantly decreases when the working temperature increases from 20 °C to 70 °C. The decrease in the Li^+ diffusion coefficient is due to the formation of a 3D network structure by hydrophobic association during sol–gel transition, which inhibits the Li^+ ion migration. Furthermore, the reversibility of thermally responsive SCs is investigated by measuring the capacitance during the electrolyte heating/cooling cycles. After multiple sol–gel–sol transition cycles, there is no significant decrease in the capacitance, indicating its practical application. Herein, the reversibility of temperature-dependent structural evolution with temperature (Fig. 2e) functions as a thermal-gated behavior and controls the migration of electrolyte ions, thus realizing the construction of the smart thermoresponsive self-adjustment SCs. Similarly, another thermal sensitive copolymer, poly(*N*-isopropylacrylamide-*co*-glycidyl methacrylate) (referred to as P(NIPAM-*co*-GMA)), was used as electrolyte for the construction of smart SCs.[37] It is observed that this electrolyte is in a solution state at room temperature due to its hydrophilic characteristics, allowing the free movement of ions. However, at high temperatures the contraction of the copolymer chains causes the electrolyte to transform into a hydrophobic state, thus preventing ion migration. This process demonstrates an effective strategy replying on temperature to design smart SCs.

Notably, most reported sol–gel transition electrolytes are liquid at room temperature, which presents numerous problems (*e.g.*, encapsulation difficulties and liquid leakage), severely limiting their performance in practical applications.[41,78] Hydrogel electrolytes are considered an effective solution to solve these problems. Furthermore, hydrogel electrolytes are also ideal for portable flexible energy storage devices. In view of this, a reversible thermo-responsive PNIPAM-*co*-*N*-methylolacrylamide (NMAM) hydrogel electrolyte was successfully

synthesized by free-radical polymerization.[22] It is noted that the discharge time of the obtained SCs based on the NMAM hydrogel electrolyte gradually decreases with the gradual increase in operating temperature from room temperature (148 s) to 70 °C (21 s), which indicates that the specific capacitance of the device drops rapidly. Its specific capacitance keeps a constant value during the heating/cooling cycle, highlighting the high reversibility of the polymer electrolyte. The temperature-dependent performance presented here is attributed to the off–on ion-transport channels of the electrolyte during the heating/cooling cycle. At room temperature, the hydrogel electrolyte surface exhibits a uniform distribution of micropores formed by interconnected molecular chains (Fig. 3a), which are approximately elliptical in shape, thus facilitating the ion transport. However, most of the micropores disappear at 70 °C (Fig. 3b), which is due to the closure of ion channels caused by molecular chain association. When the temperature returns to room temperature, the closed micropores reopen (Fig. 3c), at which point the ion transport channels are unobstructed. With a similar idea, an ionic liquid cross-

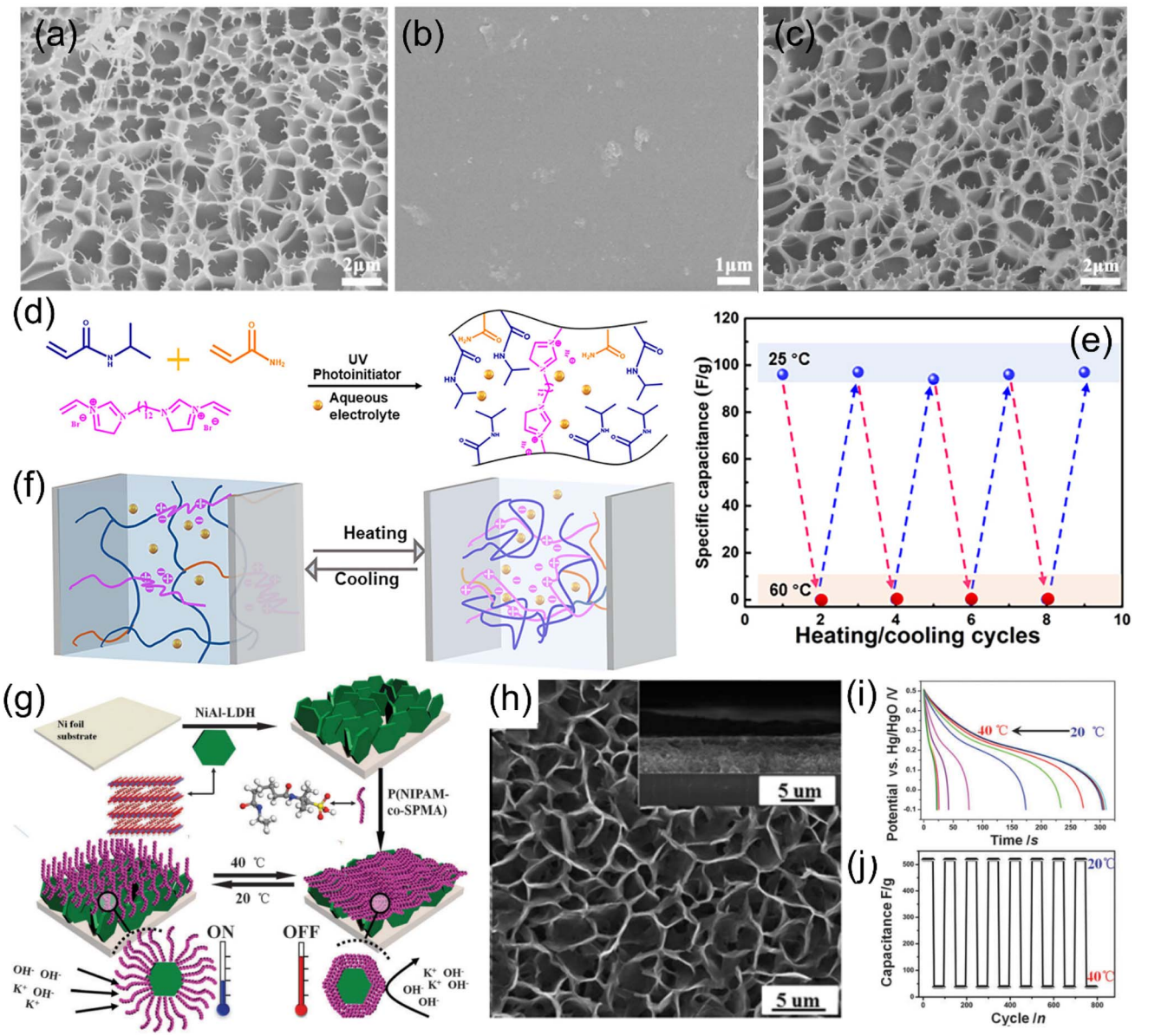

Fig. 3 Morphologies of PNIPAM/NMAM under heating/cooling cycles: (a) 25 °C, (b) 70 °C, and (c) 25 °C (cooling down), respectively.[22] Reproduced with permission.[22] Copyright 2021, American Chemical Society. (d) Illustration of the preparation of PNIPAM hydrogels through *in situ* polymerization. (e) Repeatable capacitances of SCs based on the PNIPAM hydrogel and (f) corresponding illustration of ion migrations under heating/cooling cycles.[79] Reproduced with permission.[79] Copyright 2023, American Chemical Society. (g) Illustration of the preparation of the LDH@P(NIPAM-*co*-SPMA) film electrode and its working principle towards thermal response. (h) SEM images of the LDH@P(NIPAM-*co*-SPMA) film. (i) Discharge curves of the LDH@P(NIPAM-*co*-SPMA) film electrode at different temperatures and (j) its corresponding specific capacitance during the cooling/heating process.[27] Reproduced with permission.[27] Copyright 2013, Royal Society of Chemistry.

linked PNIPAM hydrogel electrolyte was synthesized by a one-step *in situ* polymerization (Fig. 3d).[79] It is noted that the capacitance of the device is around 102 F g^{-1} at 25 °C while reducing to almost 0 at 60 °C (Fig. 3e), and the corresponding capacitance recovers when the temperature cools down to room temperature. The reversible thermoresponsive electrochemical behavior can be explained as follows. When the operating temperature is higher than the LCST value, the PNIPAM polymeric chains form physical cross-linkers, thus disrupting the original ion-conductive channels (Fig. 3f). Meanwhile, the ionic liquid component also plays an important role in confining the conductive ions in the polymer phase, thus accelerating the LCST effect on ion modulation and effectively controlling ion migrations. Undoubtedly, these two factors result in a significant decrease in the ion conductivities at 60 °C. This is supported by the diffusion coefficient of lithium ions decreasing from 5.97×10^{-11} m^2 s^{-1} at 25 °C to 2.72×10^{-13} m^2 s^{-1} at 60 °C.

Apart from the design of the thermoresponsive electrolytes, another feasible solution for the construction of thermoresponsive SCs is to directly integrate the thermoresponsive materials into electrodes from a material point of view. In view of this, a simple strategy was to load a thermosensitive polymer (*e.g.*, P(NIPAM-*co*-SPMA)) onto the surface of NiAl-layered double hydroxide (referred to as the LDH@P(NIPAM-*co*-SPMA) electrode) (Fig. 3g and h).[27] Based on the discharge curves, its specific capacitance dramatically decreases from 518 F g^{-1} at 20 °C to 38 F g^{-1} at 40 °C (Fig. 3i). The largely suppressed electrochemical capacitance at 40 °C is attributed to the closure of the ion transport channels. Also, it is noted that the specific capacitance quickly switches between 20 °C and 40 °C (Fig. 3j), indicating a highly reversible transition of this composite electrode induced by the P(NIPAM-*co*-SPMA) polymer. This thermoresponsive polymer acts as a valve by changing its configuration under cooling/heating conditions, thus promoting and preventing the diffusion of electrolyte ions. Encouragingly, this general and promising approach can be extended to design other thermoresponsive electrodes and functionalize other components, thus enabling the obtained smart devices with thermal responsibility.

3.1.2 PEO/PPO-based polymers for temperature-responsive SCs. Although the above-mentioned PNIPAM polymer-based electrolytes can be used to construct the temperature-responsive SCs, poor interfacial compatibility between the electrolyte and the electrode surface, slow response rate, and relatively low LCST negatively affect the overall capacitive performance and limit the operating temperature range of the obtained SCs as well as their practical applications. Therefore, it is necessary to explore new electrolyte systems for further improvement. Among them, devices using PEO/PPO-based polymers have shown great promise for electrolytes in the design of temperature-responsive SCs. PEO is a crucial component in creating thermoresponsive polymers, especially when combined with hydrophobic blocks like PPO, which can produce materials with tunable LCST and be used to construct temperature-responsive SCs. A representative example of such an electrolyte system is the PEO/1-ethyl-3-methylimidazolium tetrafluoroborate ([EMIM][BF_4]) composite electrolyte (Fig. 4a),[12] which is composed of an ionic liquid (IL) (here, IL refers to [EMIM][BF_4]), PEO, and Li^+ salts. As shown in Fig. 4b, the increase in charge storage of the SCs based on active carbon (AC) electrodes in pure [EMIM][BF_4] electrolyte is proportional to the working temperature. However, it is noted that its capacitance at 160 °C drops by approximately 30% compared to the value at 100 °C (Fig. 4c). These electrochemical results reveal that the L-PEO–[EMIM][BF_4] electrolyte impedes electrochemical processes at elevated temperatures because of a thermally activated phase separation in the L-PEO–[EMIM][BF_4] (50/50) electrolytes above 140 °C. Briefly, when the working temperature is above 140 °C, a PEO-rich phase is formed inside the nanopores of AC, which hinders charge accumulation at the electrode/electrolyte interface, thus leading to the decay of stored charge. Therefore, the smart responsive polymer electrolyte system shows promise for the further development of thermo-responsive SCs.

Inspired by this work, Pluronic copolymers, which are triblock copolymers with a central hydrophobic chain of PPO flanked by two hydrophilic chains of PEO, forming a PEO–PPO–PEO structure, were synthesized,[28] making them amphiphilic. The unique structure of Pluronic copolymers allows them to self-assemble in water into micelles and change from liquid to gel with increasing temperature (Fig. 4d), thus making them more attractive for the design of thermoresponsive SCs. According to the results shown in Fig. 4e, the device exhibits a relatively high specific capacitance at 20 °C, but its capacitance drops by approximately 50% at 70 °C (Fig. 4f), which is due to electrolyte gelation. Furthermore, by adjusting the concentration of the Pluronic solution from 30 wt% to 5 wt%, the transition temperature can be regulated over a wide range. This is because, when the Pluronic solution concentration decreases, the average distance between micelles becomes larger. In this case, a higher temperature is required to drive the polymer chains to become fully entangled. In addition, the capacity loss can be controlled by the molecular weights of Pluronic solutions. These adjustable properties make this electrolyte a promising candidate for the construction of smart SCs.

Due to the attractive chemical/physical properties of the Pluronic polymer mentioned above, it has been extended to explore other non-aqueous smart electrolytes and then construct smart SCs. For instance, a thermal-responsive electrolyte consisting of [EMIM][BF_4], Pluronic F127 (PEO-*b*–PPO–*b*-PEO), and lithium tetrafluoroborate ($LiBF_4$) was successfully prepared.[80] Compared with the pure $LiBF_4$ electrolyte system, the Pluronic-IL electrolyte system exhibits significantly temperature-dependent electrochemical performance (Fig. 4g and h). The SCs in a 20 wt% Pluronic–IL electrolyte delivers a capacitance of 40 F g^{-1} at 100 °C, while it only maintains about 17.6 F g^{-1} at 160 °C (a 56% loss in specific capacitance), which indicates that ion migration is significantly suppressed at high temperatures. This temperature-dependent capacitance variation is attributed to the compositional structure of Pluronic–[EMIM][BF_4] (Fig. 4i), which controls the resistance of ion migration. In this structure, the PEO segment is [EMIM][BF_4]-philic due to hydrogen bonds formed between the epoxy groups and the C2–H of the imidazole cations, and between BF^-

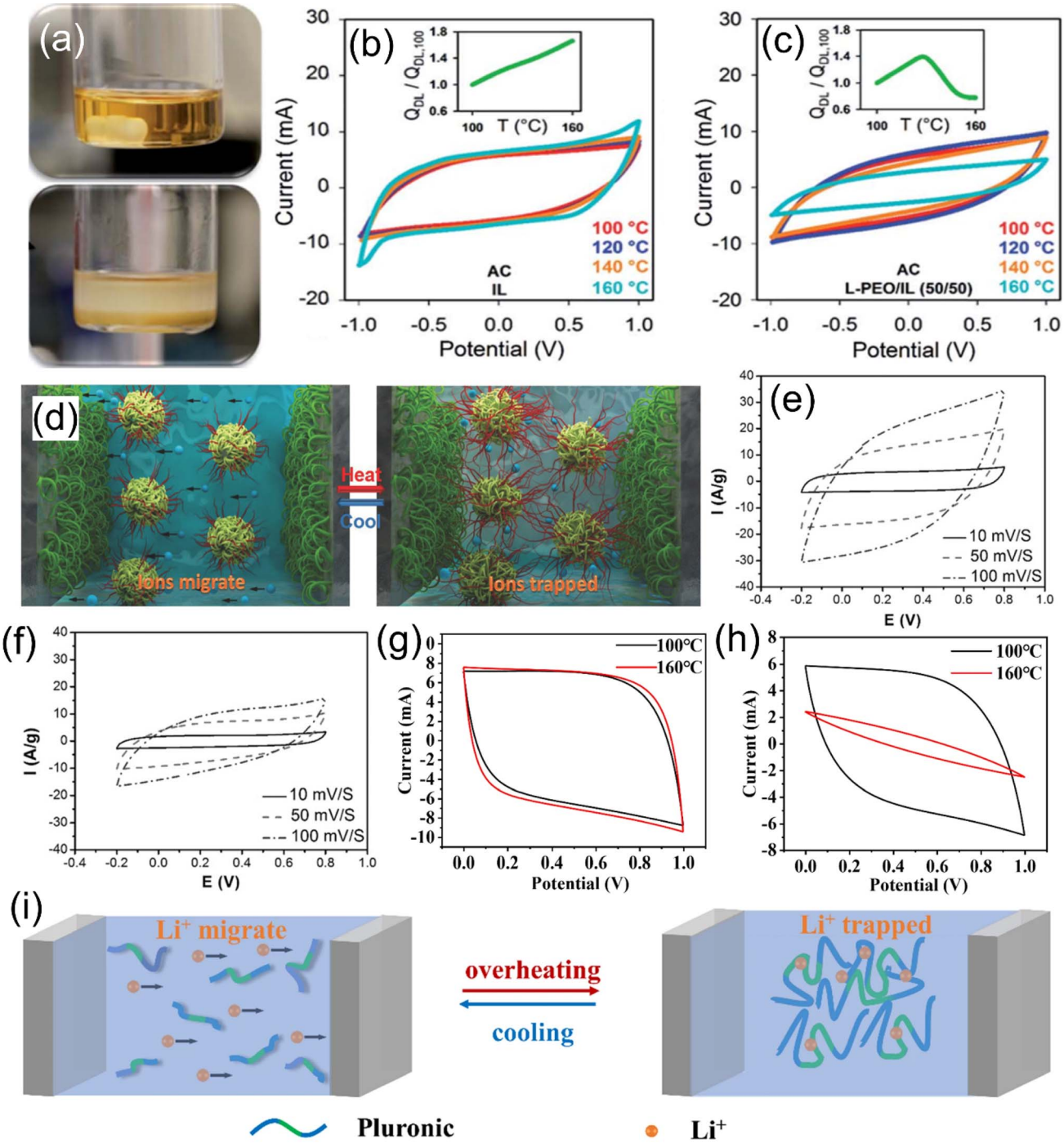

Fig. 4 (a) Photographs of the PEO/[EMIM][BF_4] mixture electrolyte at room temperature (top) and high temperature (bottom). Temperature dependence of CV profiles for AC electrodes in (b) pure [EMIM][BF_4] and (c) L-PEO/[EMIM][BF_4] (50/50) electrolytes at different testing temperatures.[12] Reproduced with permission.[12] Copyright 2015, Royal Society of Chemistry. (d) Illustration of the obtained gel electrolyte under heating/cooling cycles. The CV curves of the device using 20 wt% Pluronic solution ($M_w \approx 5800$ Da) dissolved with aqueous H_2SO_4 as the electrolyte at (e) 20 °C and (f) 70 °C, respectively.[28] Reproduced with permission.[28] Copyright 2016, Wiley-VCH. CV curves at 100 mV s^{-1} for (g) pure [EMIM]BF_4 and (h) Pluronic–[EMIM]BF_4 electrolytes with 0.01 M $LiBF_4$. (i) Illustration of the Pluronic-IL electrolyte under heating/cooling cycles.[80] Reproduced with permission.[80] Copyright 2022, Springer Nature.

and H^- at the Pluronic hydroxyl terminus. Furthermore, the PPO segment is [EMIM][BF_4]-phobic, leading to micelle formation, allowing Pluronic to be well dispersed in [EMIM][BF_4] and move freely below the transition temperature. However, above the transition temperature (≥130 °C), the hydrogen bonds between the PEO segments and the ionic liquid weaken, and the PEO segments become entangled, forming a gel electrolyte. The highly reversible sol–gel transition behavior of Pluronic–[EMIM]

[BF_4] electrolytes enables the design of energy storage devices with smart thermo-responsive properties.

3.1.3 Cellulose derivatives for temperature-responsive SCs. Clearly, the strategy of constructing temperature-responsive smart SCs through the rational design of polymer electrolytes is promising. Typically, thermoresponsive electrolytes (*e.g.*, PNIPAM-based polymers and PEO/PPO-based polymers) undergo sol–gel transition/phase separation at high temperature,[37] which suppresses ion migration and reduces ionic conductivity, thus resulting in temperature-dependent capacitive behavior in the SCs. However, these copolymers still display some drawbacks. For instance, PNIPAM-based polymers are commonly used in the design of smart SCs but are mostly limited to copolymers of NIPAM with AA or AM.[11,26,81] Furthermore, their properties are often affected by the pH of electrolyte. In addition, for the reported Pluronic electrolytes, the use of high concentrations not only increases the overall cost but also compromises the electrochemical performance.[28,37]

Considering the drawbacks mentioned above, it is necessary to explore alternative thermoresponsive electrolytes. Among them, cellulose-based derivatives have attracted attention due to their relatively high LCST and high sensitivity to temperature changes. As a representative example, a cellulose-derivative electrolyte was prepared by dissolving MC in aqueous H_2SO_4 solution (Fig. 5a).[42] It is noted that the capacitance of the AC electrode is about 90 F g^{-1} in MC/H_2SO_4 electrolyte at 25 °C while reducing to 9 F g^{-1} at 70 °C and then returning 90 F g^{-1} after cooling down (Fig. 5b). The thermal switching capacitive behavior is attributed to the adjustable ion transport of this cellulose-derivative electrolyte during the heating/cooling

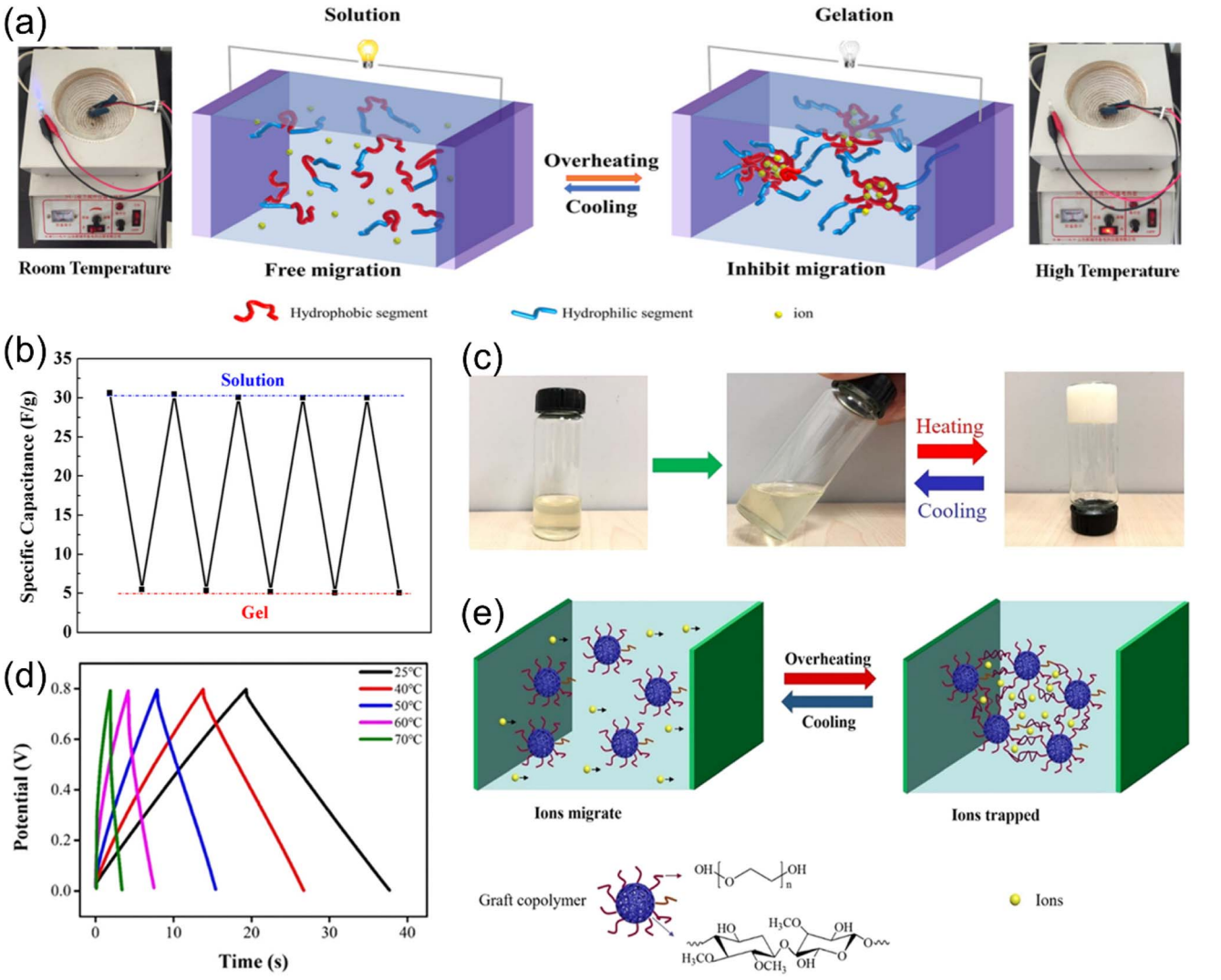

Fig. 5 (a) Illustration of the MC/H_2SO_4 electrolyte with reversible thermoresponsive properties as well as the digital photographs of the LED powered by home-made SCs based on the MC/H_2SO_4 electrolyte. (b) Capacitance of SCs based on the MC/H_2SO_4 electrolyte cycling between 25 °C and 70 °C.[42] Reproduced with permission.[42] Copyright 2018, American Chemical Society. (c) Photographs of the states of the MC-*g*-PEO copolymer electrolyte under heating/cooling cycles. (d) Charge/discharge curves of MSCs at 1 A g^{-1}. (e) Illustration of the phase transition of the MC-*g*-PEO copolymer electrolyte during the heating/cooling cycles.[43] Reproduced with permission.[43] Copyright 2019, American Chemical Society.

cycles.[42,77] Subsequently, to further optimize the application of cellulosic electrolytes in smart SCs, MC-*g*-PEO copolymer electrolytes were synthesized by the same research group using a free radical copolymerization method (Fig. 5c).[43] Notably, the resulting microsupercapacitors (MSCs) completely lose their capacitance at 80 °C while recovering to their initial value at 25 °C (Fig. 5d). The reversible thermoresponsive electrochemical performance of MSCs is due to the phase transition of MC-*g*-PEO copolymer electrolytes during heating and cooling cycles (Fig. 5e). In short, when the temperature is above LCST, a gelation process occurs, which effectively inhibits ion migration, leading to a decrease in the capacitance of MSCs. However, at room temperature, the electrolyte transforms to a solution state, allowing the electrolyte ions to migrate freely. The superior performance of MSCs based on MC-*g*-PEO thermoresponsive copolymer electrolyte provides a promising strategy for the design of smart thermoresponsive SCs and other portable microelectronic devices.[43,77] Based on the aforementioned literature and related analysis, thermoresponsive polymers can serve as a "thermal gate", resulting in a reversible switch-off/on of capacitive behavior upon heating/cooling. This reversible temperature-triggered capacitive behavior (Table 2) makes them ideal materials for designing thermoresponsive smart SCs.

3.2 Magnetic field-responsive SCs

As mentioned earlier, the advantages of magnetic field-induced magnetization are crucial for the design of magnetic field-responsive SCs. Generally, ferromagnetic materials retain their magnetization, while paramagnetic materials lose their magnetism upon removal of the applied magnetic field. Therefore, the interaction between paramagnetic materials and an applied magnetic field provides the opportunity for the design of magnetic-field-responsive SCs.[82] Currently, there are two main strategies for boosting the electrochemical performances of electrodes through external magnetic interactions: (a) integrating magnetic nanoparticles into electrodes; (b) reconstructing charge density and electric polarization. Despite considerable efforts, it is essential to systematically summarize this relevant research to better understand the origin of magnetic field-dependent supercapacitive properties, thus providing useful guidance for the design of magnetic field-responsive smart SCs.

3.2.1 Metal oxides for magnetic field-responsive SCs. Among transition metal oxides, magnetic metal oxides (*e.g.*, Fe_2O_3, Mn_3O_4, and $FeCo_2O_4$), have attracted great attention. It has been reported that the effect of a magnetic field on the performance of electrode materials is closely related to their properties (*e.g.*, magnetism and conductivity) and microstructure (*e.g.*, crystal structure, surface area, and pore size).[83] Therefore, it can be expected that magnetic metal oxides with unique magnetic properties and microstructures will exhibit a significant discrepancy in the capacitive behavior of SCs in the absence and presence of a magnetic field. Among magnetic metal oxides, Fe_2O_3 has been widely used as the electrode material for the design of magnetic field-responsive SCs. As a proof-of-concept, 2D nanoleaflet-like Fe_2O_3 was synthesized by refluxing at 95 °C for 12 h followed by heat-treatment in air (Fig. 6a).[13] The electrochemical performance of the 2D nanoleaflet-like Fe_2O_3 is investigated in a three-electrode system. It is noted that nearly a 61% increase in the specific capacitance, a 170% increase in energy density, and a ten-fold increase in power density are observed under a magnetic field compared with the counterpart without a magnetic field (Fig. 6b and c). These results clearly show that its capacitive behavior is enhanced under a magnetic field, which is attributed to the changes in the thickness of the Nernst layer and a reduction in charge transfer resistance.[13]

Like other typical magnetic metal oxides, Mn_3O_4 has also attracted great attention due to its mixed valence states and distinct crystal structure. Interestingly, a very recent study revealed that Mn_3O_4 shows an opposite magnetic field-dependent variation of specific capacitance when a magnetic field is applied. This observation seems to be contrary to other magnetic metal oxides. A question arises regarding the reason for this unusual phenomenon of the Mn_3O_4 electrode for SCs under a magnetic field. It is noted that compared with MnO_2 and other common metal oxides, Mn_3O_4 shows an increased dielectric constant under a magnetic field, indicating enhanced insulation properties. This leads to a decrease in total charge collection efficiency and specific capacitance during device operation.[84]

Table 2 Electrochemical performance comparison of temperature-responsive SCs

		Capacitance (F g^{-1})		
Electrolyte	Potential window (V)	Low temperature	High temperature	Ref.
PNIPAM-AA copolymer	0–0.7	N.A. (20 °C)	85% capacitance loss (50 °C)	11
LiOH–PNIPAM/AM	0–0.8	52.5 (20 °C)	34.0 (70 °C)	26
P(NIPAM-*co*-GMA)/H_2SO_4	−0.35–0.2	118 (20 °C)	51.9 (85 °C)	37
PNIPAM-*co*-NMAM/LiTFSI	0–0.6	242.8 mF cm^{-2} (25 °C)	34 mF cm^{-2} (70 °C)	22
PEO–[EMIM][BF_4]–LiBF_4	−1.0–1.0	N.A. (100 °C)	70% capacitance loss (160 °C)	12
Pluronic solution/H_2SO_4	−0.2–0.8	110 (20 °C)	10 (70 °C)	28
Pluronic–[EMIM][BF_4]–LiBF_4	0–1.0	40 (100 °C)	17.4 (140 °C)	80
MC/H_2SO_4 electrolyte	−0.2–0.8	90 (25 °C)	9 (70 °C)	42
MC-*g*-PEO copolymer	0–0.8	59.5 (25 °C)	0 (80 °C)	43

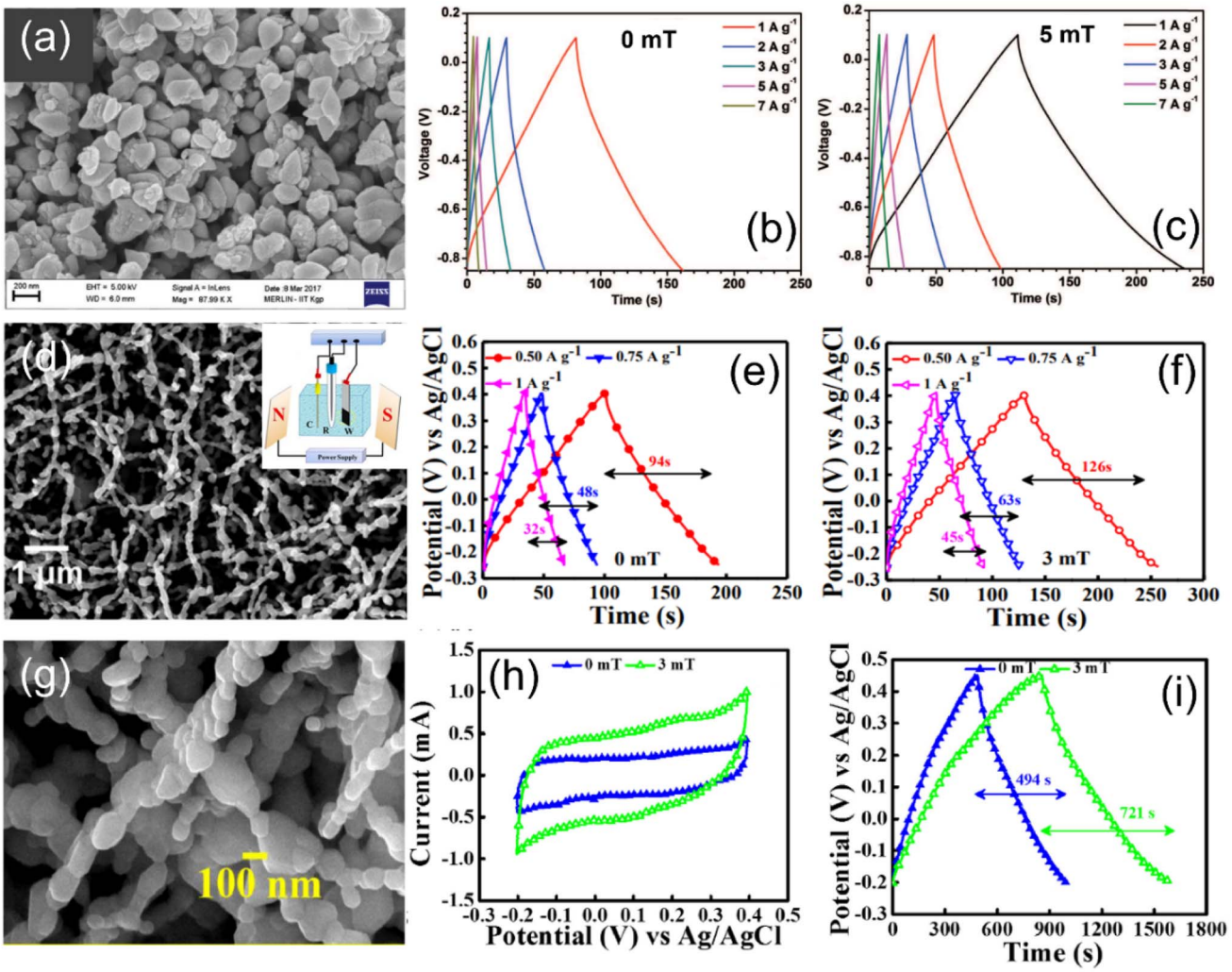

Fig. 6 (a) SEM image of nanoleaflet-like Fe_2O_3. Charge/discharge curves in the (b) absence and (c) presence of a magnetic field, respectively.[13] Reproduced with permission.[13] Copyright 2018, Wiley-VCH. (d) SEM image of the sintered $FeCo_2O_4$ nanofibers and the corresponding charge/discharge curves in the (e) absence and (f) presence of a magnetic field, respectively.[83] Reproduced with permission.[83] Copyright 2020, American Chemical Society. (g) SEM image of the sintered $FeMn_{0.2}Co_{1.8}O_4$ nanofibers and the corresponding (h) CV curves and (i) charge/discharge curves with and without of a magnetic field, respectively.[87] Reproduced with permission.[87] Copyright 2021, Elsevier.

Moreover, the energy storage performance of metal oxides is closely related to surface area, shape, and size.[29,85] Therefore, controlling the surface area, shape, and pore size is an effective strategy for boosting the capacitive behavior of electrode materials. Particularly, metal oxide nanofibers with a one-dimensional, high aspect ratio, and porous structure are considered attractive materials.[83,86] In this context, $FeCo_2O_4$ nanofibers were fabricated by the electrospinning technique (Fig. 6d).[83] Notably, after applying a magnetic field (3 mT), the capacitance of the $FeCo_2O_4$ nanofibers increases by about 34% at 0.5 A g^{-1} (Fig. 6e and f). The performance improvement is primarily attributed to the effect of the magnetic field on its bulk resistance and magnetoresistance. Clearly, the applied magnetic field enhances the overall effective field acting on the local spin and reduces spin fluctuations, thereby reducing electron–spin scattering and ultimately leading to a decrease in the bulk resistance of the $FeCo_2O_4$ nanofibers. Additionally, both Lorentz force and magnetic gradient force act simultaneously and play a crucial role in regulating ion/electron movement during charging and discharging processes.[83]

Furthermore, doping suitable metal elements into spinel-structured ferrites has been proven to change their magnetism. Thus, an identical approach is used to improve the capacitance values of the given material. Knowing this, the same group doped Mn into $FeCo_2O_4$ nanofibers (Fig. 6g).[87] The capacitive behavior of the Mn-doped $FeCo_2O_4$ nanofiber electrode is studied with and without a magnetic field. The specific capacitance of $FeMn_{0.2}Co_{1.8}O_4$ at 3 mV s^{-1} is 306 F g^{-1} under a magnetic field (Fig. 6h), which is much higher than that of the $FeMn_{0.2}Co_{1.8}O_4$ electrode (212 F g^{-1}) without a magnetic field. Surprisingly, a 46% capacitance increment is observed for the $FeMn_{0.2}Co_{1.8}O_4$ electrode under a magnetic field (3 mT) based on the charge/discharge curves (Fig. 6i), which are consistent with the results of CV curves. The excellent performance of the

$FeMn_{0.2}Co_{1.8}O_4$ electrode in an external magnetic environment is mainly due to the increase in the conductivity induced by Mn doping and the gradient force created by the magnetic susceptibility. The doping of Mn into $FeCo_2O_4$ can lower its internal resistance, while the induced gradient force can reduce the thickness of the Nernst layer and favor the ion and electronic transport at the electrode/electrolyte interface. This study shows a novel strategy for improving the capacitive behavior of electrode materials by doping appropriate elements and applying an external magnetic field.[87]

3.2.2 Nanocomposites for magnetic field-responsive SCs. Magnetic metal oxides are promising electrode materials for SCs due to their high pseudocapacitance but often suffer from unsatisfactory power density and poor cycling stability. As an alternative strategy, composite materials are commonly used as electrode materials for SCs. This is because the high conductivity and stability of one material, combined with the high capacitance value of another, create a synergetic effect, thus improving electrochemical performance.[88] From this perspective, researchers have tried to boost performance by preparing nanocomposites, which typically involves incorporating magnetic metal oxides with conductive polymers or different types of carbon materials, thus achieving a trade-off between high capacitance and good cycle stability. In this sense, coupling the magnetic metal oxides with conductive polymers is a feasible strategy to overcome the above-mentioned issues and achieve enhanced performance. Fe_3O_4/PPy nanocomposites were fabricated *via* a simple surface-initiated polymerization method.[89] The Fe_3O_4/PPy nanocomposite display enhanced capacitive behavior. Particularly, under a magnetic field, its energy density is 10 times higher than that of its counterparts without a magnetic field. With a magnetic field, the movement of electrolyte ions is accelerated by an additional Lorentz force. Undoubtedly, with a magnetic field, faster-moving ions can more efficiently compensate for the ions consumed in redox reactions, thus contributing to electrochemical performance improvement.[89]

Recently, the combination of advanced carbon materials with magnetic metal oxides has also attracted considerable interest.[90,91] For instance, a MnO_2/carbon nanofiber composite was fabricated by electrospinning followed by electrochemical deposition (Fig. 7a–d).[92] The electrochemical performance of the MnO_2/carbon nanofiber composite with and without a magnetic field is investigated (Fig. 7e). With an applied magnetic field, the MnO_2/carbon nanofibers show magneto-enhanced performance in terms of higher charge density, longer discharge time and lower internal resistance, indicating the magneto-enhanced capacitor performance. The enhancement is attributed to the fast electron transfer reaction arising from the magnetic susceptibility-induced electron spin of MnO_2, the fast mass transport, and the improved cation intercalation/de-intercalation.[92] As another representative example, an AC/Fe_3O_4 nanocomposite was synthesized *via* a simple hydrothermal method followed by ultrasonication.[93] Its electrochemical performance is investigated under magnetization and non-magnetization conditions. Encouragingly, the capacitive behavior of the AC/Fe_3O_4 nanocomposite is boosted with the implementation of a magnetic field, which is due to the magnetic field improving ion/electron transport and reducing charge transfer resistance. Specifically, under magnetization conditions, the introduction of Lorentz force improves the transportation efficiency of the electrons, and the change in the microscopic structure of the electrolyte molecules enhances the electrical conductivity of the electrolyte, thus contributing to the improvement of supercapacitive performance.[93] Similarly, a graphene/Fe_2O_3 nanocomposite was fabricated by facile thermal decomposition (Fig. 7f).[91] Notably, the graphene/Fe_2O_3 nanocomposite electrode shows 92.5% specific capacitance enhancement in the presence of a magnetic field (Fig. 7g and h). Moreover, the corresponding energy and power densities are also enhanced in the presence of a magnetic field, which is attributed to the significant restriction of the interfacial relaxation process. This work presents a new and effective strategy for improving the capacitive behavior under a magnetic field and for constructing magnetic-responsive SCs.[91]

Up to now, many efforts have been made to design magnetic metal oxide-based electrodes, which display obvious magnetic-induced capacitive behavior. However, it is still a great challenge to explore a simple and universal strategy for the synthesis of magnetic metal oxides with significant enhancement of capacitive behavior. Taking this into account, a general approach was proposed to synthesize magnetic metal oxide-based hybrid materials. A series of metal oxides (*e.g.*, NiO, Co_3O_4, and Fe_3O_4)/nitrogen-doped graphene (NG) composites were synthesized by *in situ* deposition of magnetic metal oxides on nitrogen-doped graphene.[94] The electrochemical performance of these hybrid electrodes is evaluated without and with an external magnetic field. Here, taking Fe_3O_4/nitrogen-doped graphene (Fe_3O_4/NG) as example, the effect of an applied magnetic field on the capacitive behavior is investigated (Fig. 7i). The results show that the capacitance of Fe_3O_4/NG increases by about 28.8% after applying a magnetic field compared to the state without a magnetic field (Fig. 7j and k). Furthermore, Fe_3O_4/NG also exhibits a longer discharge time with a magnetic field compared to its counterpart (Fig. 7l and m), indicating improved performance, consistent with the results of CV curves. These electrochemical results demonstrate that the magnetic field plays a crucial role in the charge/discharge process of the Fe_3O_4/NG electrode. Clearly, the magnetic field significantly enhances the charge carrier transportation through the Lorentz force, thus promoting electrolyte convection and enhancing ion transport. In addition, the magnetic field can reduce the interfacial resistance by decreasing charge transfer resistance and increasing the charge transport efficiency between the electrode and the electrolyte. In a word, the improved ion transport, the increased interface charge density, and the reduced resistance enhance the capacitive behavior.[94]

According to the above discussion, the electrochemical performance of SCs can be effectively regulated by a magnetic field (Table 3). In short, the capacitive behavior of the electrode materials is improved with a magnetic field due to the increase of electron transportation efficiency. Furthermore, the Lorentz force acts on moving charges/ions in the electrolyte and leads

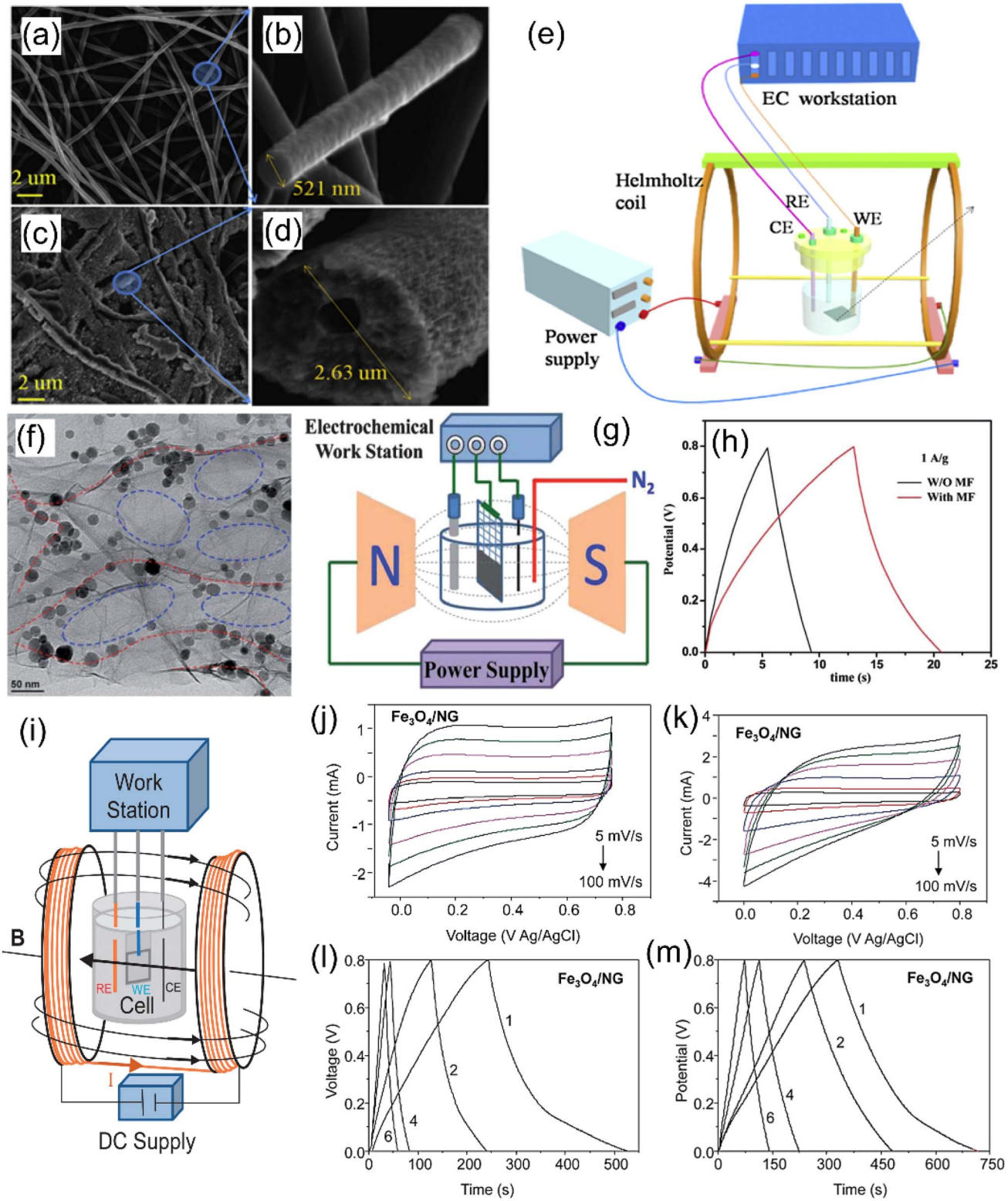

Fig. 7 SEM images of (a) and (b) pure carbon fiber and (c) and (d) MnO_2/carbon fiber, respectively. (e) Illustration of the electrochemical setup for a MnO_2/carbon fiber electrode tested under an external magnetic field.[92] Reproduced with permission.[92] Copyright 2017, Elsevier. (f) TEM image of graphene/Fe_2O_3 nanocomposites. (g) Illustration of the capacitive behavior of graphene/Fe_2O_3 tested in a magnetic field and (h) corresponding charge/discharge curve.[91] Reproduced with permission.[91] Copyright 2013, Royal Society of Chemistry. (i) Schematic diagram of the electrochemical performance of Fe_3O_4/nitrogen-doped graphene conducted in the presence of an external magnetic field. (j) and (k) CV curves and (l) and (m) charge/discharge curves of the Fe_3O_4/nitrogen-doped graphene with and without a magnetic field.[94] Reproduced with permission.[94] Copyright 2020, Oxford University Press.

Table 3 Electrochemical performance comparison of magnetic field-responsive SCs

Electrode material	Electrolyte	Potential window (V)	Capacitance (F g^{-1}) Without a magnetic field	With a magnetic field	Ref.
2D nanoleaflet-like Fe_2O_3	1 M KOH	−0.85–0.1	86 (1 A g^{-1})	134 (1 A g^{-1})	13
Mn_3O_4	1 M Na_2SO_4	0–1.0	208 (1 A g^{-1})	156 (1 A g^{-1})	84
$FeCo_2O_4$ nanofibers	2 M KOH	−0.25–0.4	106 (3 mV s^{-1})	165 (3 mV s^{-1})	83
$FeMn_{0.2}Co_{1.8}O_4$	2 M KOH	0–0.6	212 (3 mV s^{-1})	306 (3 mV s^{-1})	87
Fe_3O_4/PPy nanocomposite	1 M H_2SO_4	−1.2–0.8	332.9 (1 A g^{-1})	413.8 (1 A g^{-1})	89
MnO_2/carbon nanofiber composite	6 M KOH	0–0.8	114 (1 A g^{-1})	180 (1 A g^{-1})	92
AC/Fe_3O_4 nanocomposite	6 M KOH	−1.0–0	136 (1 A g^{-1})	105 (1 A g^{-1})	93
Graphene/Fe_2O_3 nanocomposite	1 M Na_2SO_4	−1.0–1	208 (1 A g^{-1})	156 (1 A g^{-1})	91
Fe_3O_4/nitrogen-doped graphene	1 M NaCl	0–0.8	5.4 (1 A g^{-1})	8.6 (1 A g^{-1})	94

the electrolyte ions to move in a circular pattern towards the electrode surface, thereby causing electrolyte convection and reducing the resistance of the bulk electrolyte. Meanwhile, this magnetohydrodynamic effect pushes the electrolyte ions to reach extra electrode surface area, which cannot be accessed without applying the magnetic field. In a word, the tunable capacitive behavior under a magnetic field could be a promising strategy for the design of magnetic-responsive SCs.

3.3 Photo-responsive SCs

Photo-responsive SCs are another new type of smart SCs, in which the incorporation of electrode materials with light-responsive properties provides the resulting SCs with photo-responsive characteristics and enhanced capacitive behavior. In this device, the photoactive materials (*e.g.*, conducting polymers, metal sulfides, and metal oxides) absorb light to generate electron–hole pairs,[95] which then drive fast surface redox reactions or form a double-layer capacitor. Therefore, the development of optically driven SCs requires electrode materials that enable both photogenerated electrons and holes to be internally separated. Undoubtedly, the rational design and construction of light-responsive electrodes are important factors in achieving excellent capacitive performance.

3.3.1 Conducting polymers for photo-responsive SCs. So far, scientists have made many efforts to explore novel photo-responsive positive electrodes (*e.g.*, conducting polymers, metal sulfides, and metal oxides). Particularly, by using different synthesis methods to design and prepare the photo-responsive materials with controllable morphology and structure, the as-prepared SCs exhibit good photo-responsiveness and light-enhanced supercapacitive behavior. Among these developed photo-responsive electrodes, conducting polymers with an extended π-electron system in their backbone have attracted tremendous attention. Conducting polymer photo-responsive electrodes offer several advantages for photo-enhanced SCs (*e.g.*, narrower bandgaps, high charge carrier mobility, and tunable electrical properties). Furthermore, the electrical and optical properties of conducting polymers can be tuned by adjusting the synthesis methods, optimizing the parameters, and forming composites with other nanomaterials. Additionally, the conducting polymers possess inherent flexibility, lightweight, and low cost, making them attractive candidates for wearable SCs.

Regarding these reported polymers, boron-dipyrromethene (BODIPY) and its derivatives are widely used in many fields (*e.g.*, optoelectronics, photocatalysis, and molecular sensing) due to their exceptional photophysical and chemical properties.[96] Recently, there has been growing interest in incorporating BODIPY into redox-active porous frameworks to simultaneously harvest light energy and store charge. Here, a cross-linked thieno[3,2-*b*]thiophene–BODIPY porous polymer, synthesized by using the thiol–ene click chemistry method (Fig. 8a and b), was employed as the electroactive material for the design of light-responsive SCs (Fig. 8c).[14] The extended conjugation in this BODIPY-derived porous polymer not only provides a broad absorption spectrum, but also enables a low optical bandgap, thereby facilitating light harvesting and charge transport. Obviously, there is a significant increase in discharge time (Fig. 8d) and specific capacitance (Fig. 8e) under visible light illumination, attributed to the good photo-induced charge separation and enhanced carrier mobility. Moreover, the BODIPY-derived polymer electrode also exhibits remarkable cycle stability with about 90% capacitance retention after 2000 cycles under light illumination (Fig. 8f), indicating its robust structural stability. The unique framework structure along with remarkable physicochemical properties enables the BODIPY-derived porous polymer to improve chemical stability and favor efficient photoinduced charge transport under illumination, thus boosting the capacitive behavior.[14]

Lately, the same group used a similar thiol–ene click reaction method to cross–link donor–acceptor building blocks on a graphene sheet substrate,[97] thus enabling the resulting porous organic polymer for electrode materials of photo-responsive SCs. This photoactive polymer electrode shows a capacitance of 304.1 F g^{-1} (at 2.0 A g^{-1}) and an energy density of 60 Wh kg^{-1} under visible light, which is almost two times higher than that under dark conditions. Meanwhile, the obtained polymer electrode exhibits excellent cycling stability. The remarkable performance of the photoactive polymer presented here reveals that combining donor–acceptor engineering with thiol–ene

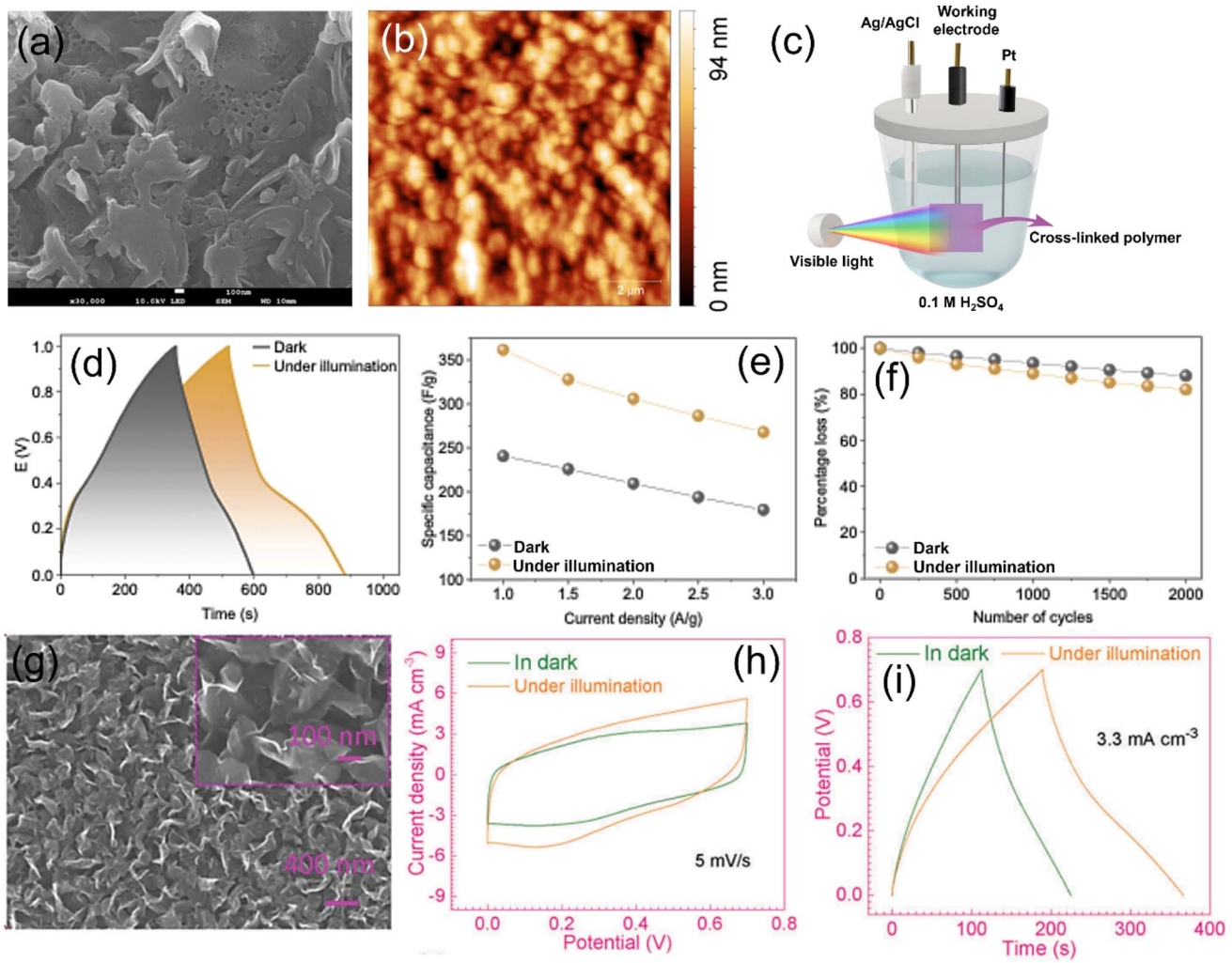

Fig. 8 (a) SEM and (b) AFM images of the BODIPY-derived porous polymer. (c) Photo-assisted three-electrode electrochemical cell configuration and its corresponding, (d) charge–discharge curves, (e) specific capacitance under different current densities, and (f) cycle stability.[14] Reproduced with permission.[14] Copyright 2025, American Chemical Society. (g) SEM images of the 3D-graphene support. (h) CV curves and (i) charge/discharge curves of the SCs based on 3D-graphene coated PEDOT:PSS electrodes in the dark and under illumination.[98] Reproduced with permission.[98] Copyright 2018, Royal Society of Chemistry.

click reaction is an effective strategy for constructing photo-assisted SCs with improved electrochemical performance.[97]

However, pure conducting polymer electrodes suffer from some drawbacks, such as unsatisfactory stability, relatively low electronic conductivity, and poor electron–hole separation. Therefore, the design of conducting polymer composite is considered as another effective strategy to enhance the capacitive behavior. For instance, a photoresponsive pseudo-capacitor was assembled with 3D graphene (Fig. 8g) coated with a PEDOT:PSS electrode.[98] Interestingly, compared with the device tested in the dark, the device displays a larger area surrounded by the CV curve (Fig. 8h), a longer discharge time (Fig. 8i), and a larger volumetric capacitance, demonstrating a significant improvement in capacitive performance under solar illumination. Notably, the enhancement of the capacitive behavior of the device under illumination is due to the photo-induced effect, which increases the electrode conductivity and the reaction rate constant. In addition, the strategy can be extended to other materials with high light thermal conversion efficiency.[98]

3.3.2 Metal sulfides for photo-responsive SCs. Owing to their intermediate to narrow band gaps, good electrical conductivity, high ionic diffusivity, and high specific capacitance, metal sulfides are also considered excellent pseudo-capacitive candidates for the construction of photo-responsive SCs. As an example, a light-induced SC was built with vertically aligned ReS_2 nanosheets grown on conducting substrates *via* chemical vapor deposition (Fig. 9a).[30] The vertically aligned ReS_2 nanosheet electrode (Fig. 9b) shows a larger area enclosed by the CV curve than the counterpart (Fig. 9c), demonstrating increased charge storage under light illumination. Also, the ReS_2 nanosheet electrode possesses a longer discharge time and a higher volumetric capacitance under a series of current densities with the presence of light (Fig. 9d). The

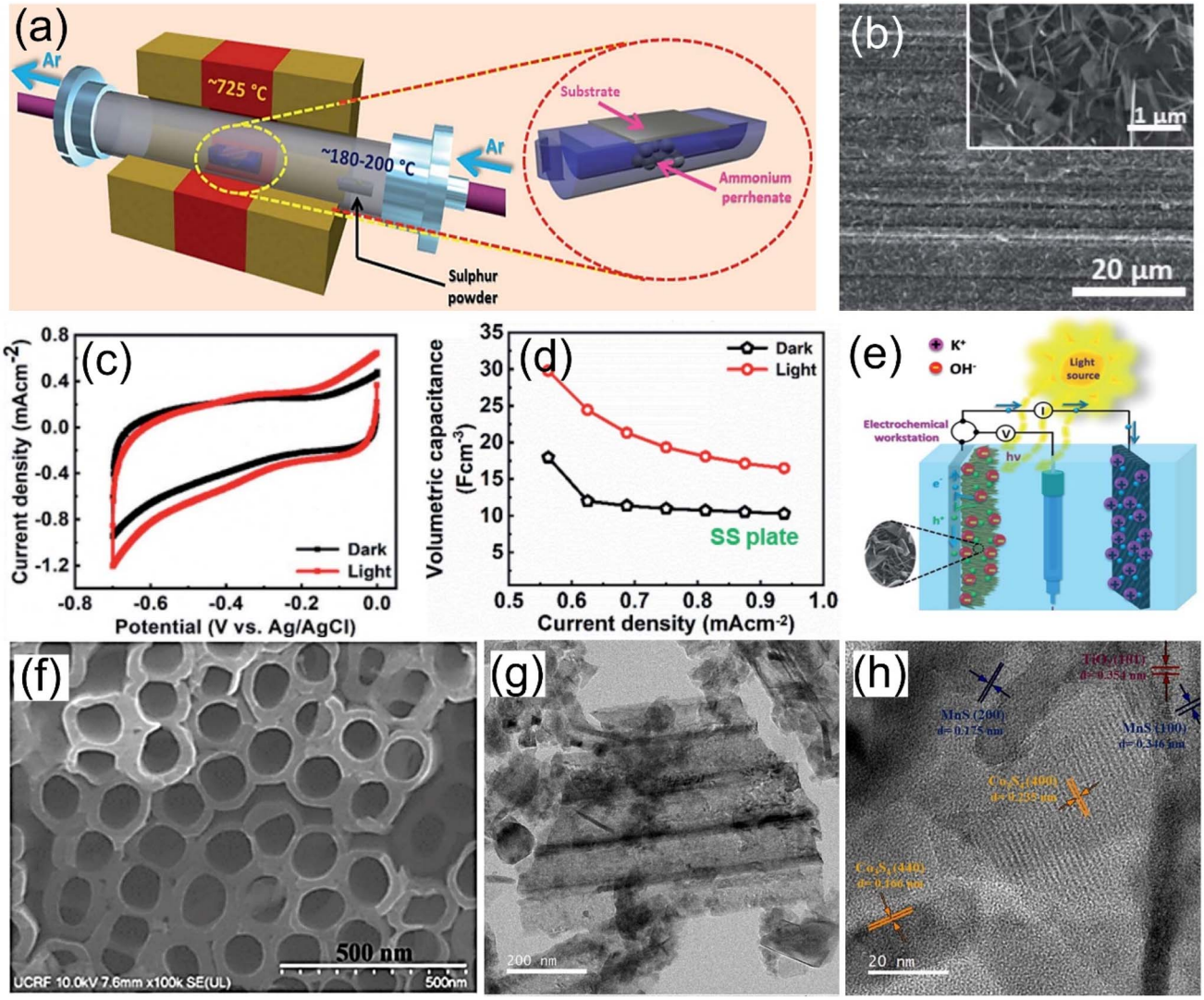

Fig. 9 (a) Illustration of growth of ReS_2 *via* the CVD method, (b) SEM images of ReS_2 grown on stainless steel. (c) CV curves of the ReS_2 electrode at 100 mV s^{-1} under dark and light conditions. (d) Rate capability of the ReS_2 electrode under dark and light conditions. (e) Illustration of the mechanism of light-induced energy storage in ReS_2.[30] Reproduced with permission.[30] Copyright 2021, Royal Society of Chemistry. (f) SEM image of CoMnS decorated on TiO_2 nanotubes and corresponding (g) low-resolution and (h) high-resolution TEM images.[99] Reproduced with permission.[99] Copyright 2024, Elsevier.

supercapacitive performance enhancement is due to the generated electron–hole pairs under light illumination (Fig. 9e), which favor charge storage. Briefly, when light is induced, the ReS_2 nanosheets absorb light and generate electron–hole pairs. Then, the generated electron–hole pairs, separated by the applied potential, provide extra charge carriers, thus allowing more electrolyte ions to accumulate at the electrode/electrolyte interface and contributing to the enhancement of capacitive behavior.[30]

Furthermore, bi-/ternary metal sulfides are also promising candidates as photo-electrodes for photo-assisted SCs due to their desirable optimal band gap, higher absorption coefficient, and higher capacitance compared with mono-metal sulfides. Binary CoMnS decorated on TiO_2 nanotubes (Fig. 9f–h) were prepared as photoelectrodes for photo-assisted SCs.[99] Based on the testing results, the photo-assisted SCs can simultaneously harvest light and effectively store charge to provide enhanced capacitive behavior in terms of prolonged discharge time, capacity enhancement (70% increment), and good cycle life under light irradiation.[99] In addition, ternary Cu_2ZnSnS_4 synthesized by a simple and mild solvothermal reaction was employed as a photo-electrode for the construction of photo-assisted SCs.[100] It was noted that with light irradiation, the optimized Cu_2ZnSnS_4 electrode displays a significant enhancement in capacitive behaviour including a larger area enclosed by the CV curve, a higher specific capacitance, and a lower interfacial charge transfer resistance in comparison to the dark conditions.

3.3.3 Metal oxides for photo-responsive SCs. Apart from conducting polymers and metal sulfides, metal oxides are widely employed to fabricate light-responsive smart SCs with enhanced energy storage performance. Metal oxides (*e.g.*, TiO_2,

ZnO, Fe_2O_3, are V_2O_5) are well-known semiconductors that can absorb ultraviolet light and generate electron–hole pairs. In photo-enhanced SCs, the internal electric field helps separate the photo-generated charges. This effectively increases the number of charge carriers available for the electrochemical reactions, resulting in enhanced capacitive behavior compared to the metal oxide electrodes tested in the absence of light. Moreover, nanoengineering metal oxides into various forms, morphologies, and structures can also enhance the performance of as-prepared photo-responsive SCs by boosting the rate of photo-assisted charge transfer reactions, increasing the interaction between active material and electrolyte, and facilitating ion diffusion.

As one of the commonly used metal oxides, WO_3 with a narrow band gap can not only absorb visible light to generate electron–hole pairs but also react with some small cations to form tungsten bronze, thus exhibiting a unique photochromic property. In this case, WO_3 is expected to be a promising candidate material for designing photo-responsive SCs. As a proof-of-concept, WO_3 synthesized by using a microwave-assisted hydrothermal method served as a photo-electrode for the construction of photo-responsive SCs (Fig. 10a).[101] The electrochemical performance of WO_3-based SCs is improved under solar light, as evidenced by an increase in the area surrounded by the CV curve (Fig. 10b) and a prolonged discharge time based on the charge/discharge curves (Fig. 10c). According

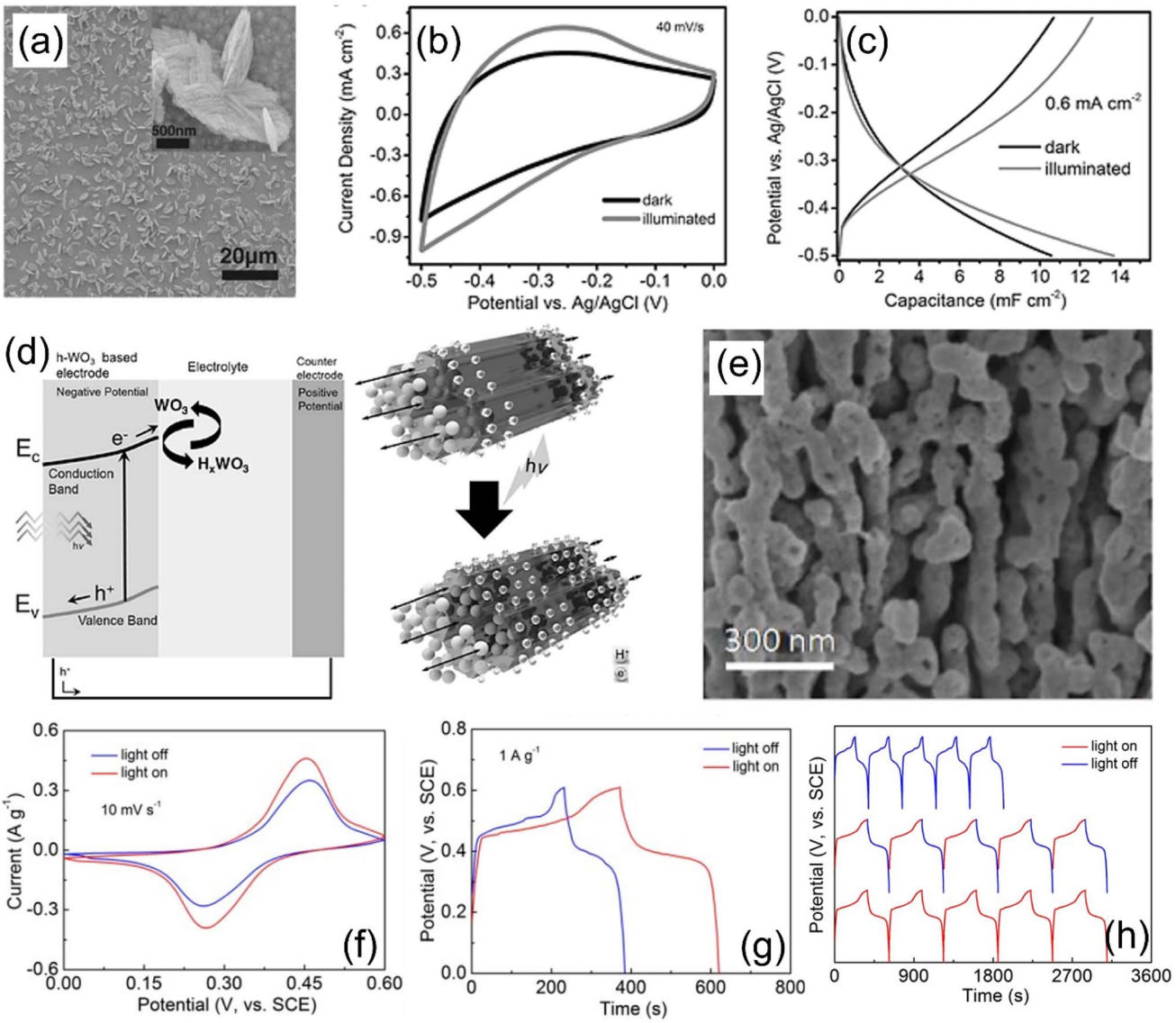

Fig. 10 (a) SEM image of h-WO_3 films grown on fluorine-doped tin oxide (FTO). (b) CV curves and (c) charge/discharge curves of the obtained h-WO_3 film electrode under dark conditions and under illumination with solar light, respectively. (d) Illustration of the increase in capacitance for h-WO_3 film electrodes under solar light illumination.[101] Reproduced with permission.[101] Copyright 2016, Wiley-VCH. (e) SEM image of 3D nanoporous Cu@Cu_2O composite electrodes. (f) CV curves and (g) charge/discharge curves of the 3D nanoporous Cu@Cu_2O electrode under dark conditions and light illumination. (h) Charge/discharge profiles of the 3D nanoporous Cu@Cu_2O electrode under dark conditions and light illumination.[102] Reproduced with permission.[102] Copyright 2019, Royal Society of Chemistry.

to the energy storage kinetic analysis, the photoexcited electrons not only facilitate the insertion of protons into WO_3 during charging but also accelerate the discharging kinetics. The specific effect of light illumination on the capacitive behavior of the WO_3-based SCs can be explained as follows (Fig. 10d). When the WO_3-based electrode is exposed to light and absorbs the light energy, electron–hole pairs are generated at the same time. During the charging process, the generated electrons are transferred to the electrode/electrolyte interface; subsequently they cause the reduction of WO_3 accompanied by the insertion of protons. In contrast, during the discharge process, the stored electrons are released, and the inserted protons are extracted back into the electrolyte, corresponding to a reversible proton-coupled electron storage process. Therefore, the kinetics of the charging/discharging process of the WO_3-based SCs can be sped up under light irradiation.[101]

Moreover, the performance of metal oxides can be improved through various strategies such as preparing composites, which can facilitate the electron–hole pair separation and allow more efficient absorption of visible light. As a representative example, the Mn_3O_4/rGO composite exhibited an 82% increase in capacitance under light conditions compared to that under dark conditions.[49] The increment in capacitance is mainly due to the photoexcitation of electrons when an external light source was applied. In brief, when an external light source irradiates the active region of the electrode, the electron–hole pairs are separated during the charge/discharge process, thus accelerating the photo excitation and enhancing the capacitance.[49] Furthermore, nanoengineering metal oxides with specific morphology and structures is also conducive to boosting the performance of as-prepared photo-responsive SCs. In view of this, a photo-responsive SCs was constructed using a 3D nanoporous Cu@Cu_2O array (Fig. 10e) as the working electrode.[102] Electrochemical results show that, with the aid of solar light, the current densities of redox peaks in the CV curves increase (Fig. 10f), and the voltage difference between the oxidation and reduction peaks decreases, indicating enhanced capacitance and improved reversibility. Also, it is noted that the device exhibits a lower charge voltage plateau, a higher discharge plateau, and a longer discharge time (Fig. 10g), further demonstrating the improved reversibility and enhanced capacitance under light illumination. Furthermore, the comparative experiment (Fig. 10h) shows that light significantly affects the charging process. The mechanism underlying the performance improvement of the 3D nanoporous Cu@Cu_2O electrode under solar light illumination is briefly described as follows. Under light illumination, the semiconductor Cu_2O generates electron–hole pairs, in which the photo-generated holes oxidize Cu_2O to CuO, while the photo-generated electrons pass through the external circuit and produce H_2 by reduction reaction. The corresponding discharge process is the inverse procedure. Herein, the 3D nanoporous Cu@Cu_2O electrode design provides a new solution for the construction of photo-responsive energy storage devices.[102]

Although photo-active electrode materials can generate electron–hole pairs under light illumination, carrier separation is very important for the generated carriers to reach the electrode where they are collected. In this case, minimizing the recombination rate can achieve better device performance. As reported, interface design is a better option to reduce the recombination rate of the photo-active electrode. In this way, the design of heterojunction photoresponsive electrodes, especially type II heterojunctions,[103] is able to offer significant performance enhancements over single-material electrodes, primarily by improving the efficiency of charge separation and transport. First, a built-in electric field formed at the interface between two different materials acts as a driving force to separate the electron–hole pairs, thus significantly suppressing their recombination and ensuring that more carriers participate in the reactions. Second, the heterojunction electrodes can absorb light over a wider range of the electromagnetic spectrum, enabling more efficient utilization. Hence, a bi-layer TiO_2/MoO_3 heterojunction electrode was designed with a simple sol–gel and spin coating method (Fig. 11a, b).[104] The typical CV curves of the TiO_2/MoO_3 heterojunction electrode reveal faster redox reaction and larger energy storage capability under UV illumination. The enhanced kinetics under light illumination can be briefly described as follows. When the TiO_2/MoO_3 electrode absorbs light, electron–hole pairs are generated. Subsequently, the generated carriers are effectively separated under the internal driving force, whereby the generated electrons transfer to the surface of the electrode while the holes move towards the counter electrode and are then neutralized by the proton. Obviously, light illumination has a significant impact on the diffusion-controlled process (proton insertion and charge carrier separation) rather than the surface (proton) adsorption process.[104] Similarly, a carbon fiber paper-supported CeO_2/MnO_2 heterojunction electrode was successfully synthesized by a two-step *in situ* growth process.[105] Encouragingly, the obtained CeO_2/MnO_2 electrode not only displays enhanced capacitive behavior (303 F g^{-1} at 0.25 A g^{-1}) and good cycling stability but also maintains 56% of the light-enhanced capacitance even after half a day of light irradiation. The photo-induced capacitance enhancement is attributed to the well-designed CeO_2/MnO_2 heterojunction, which not only offers additional photo-induced charge carriers under light irradiation, but also facilitates charge carrier separation, thus improving its photo-assisted charging capability.[105]

As reported, the unique 3D structure facilitates efficient electron–hole separation, thus allowing the charge carriers to be used for energy conversion.[106,107] Importantly, the 3D structure provides interconnected charge transport channels, thus promoting the migration of carriers. Moreover, the high surface area increases the number of active sites and enhances light absorption. Given this, the design and preparation of 3D structural electrodes is able to boost the capacitive behavior of the device compared with that based on electrodes of other dimensionalities. As a representative example, ZnO/$ZnCo_2O_4$ nanoarrays (Fig. 11c–e) were prepared using a hydrothermal method to serve as the photo-active electrodes of SCs (Fig. 11f).[108] Under UV light exposure, the increased area enclosed by the deviated rectangular CV curve indicates the enhanced capacitive behavior and the existence of fast surface redox reactions on this electrode. Furthermore, the increased

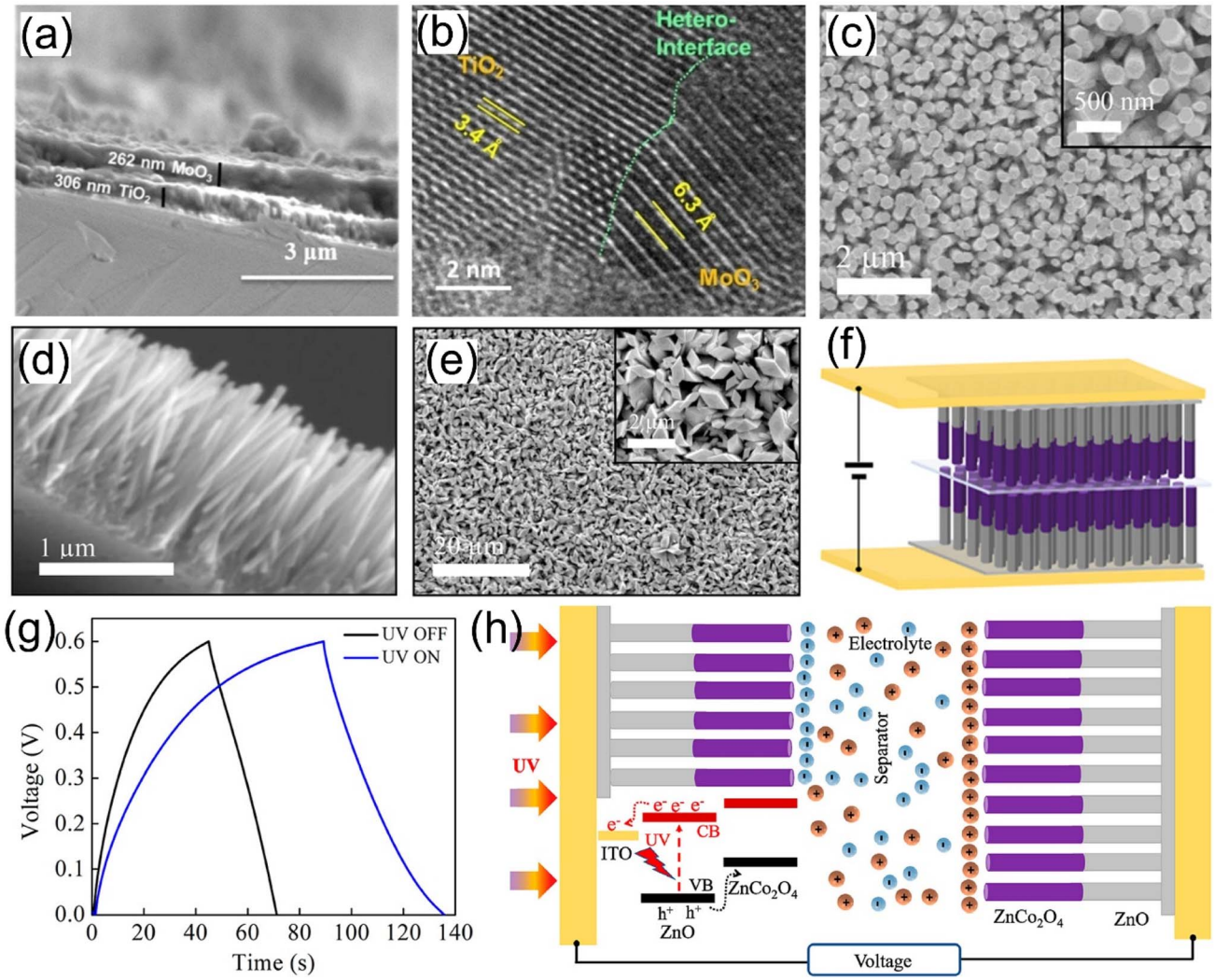

Fig. 11 (a) Cross-sectional SEM image and (b) TEM image of CeO_2/MnO_2 heterojunctions.[104] Reproduced with permission.[104] Copyright 2025, Wiley-VCH. (c) SEM image of as-grown ZnO nanoarrays. (d) Cross-sectional SEM image and (e) corresponding low and high magnification SEM images of the $ZnO/ZnCo_2O_4$ nanoarrays. (f) Illustration of the assembled SCs based on two $ZnO/ZnCo_2O_4$ nanoarrays. (g) Charge/discharge curves of the obtained SCs with and without UV light. (h) Illustration of the mechanism of the photo-responsive SCs based on $ZnO/ZnCo_2O_4$ nanoarrays under UV light.[108] Reproduced with permission.[108] Copyright 2019, American Chemical Society.

discharge time in the presence of UV exposure further confirms the enhancement of capacitance (Fig. 11g). The working mechanism of the device under UV exposure is shown as follows (Fig. 11h). Under UV illumination, the photo-generated electrons transfer from ZnO to indium tin oxide (ITO) and pass through the external circuit, while the generated holes move from ZnO to $ZnCo_2O_4$ due to the internal electric field in the heterojunctions. Subsequently, electrons at the negative electrode promote the formation of an electrical double layer at the $ZnO/ZnCo_2O_4$ electrode/electrolyte interface, while the holes at the positive electrode participate in surface-related reactions and the formation of the electrical double layer. Therefore, it can be concluded that the exposure of $ZnO/ZnCo_2O_4$ under UV light can improve electron transport efficiency and enhance the charge storage capacity of the electrode.[108] Based on the above analysis, the strategies proposed in this section provide new insights into the design of high-performance photoresponsive smart SCs (Table 4), which are expected to be applied in next-generation energy storage devices. Meanwhile, the photo-induced capacitive enhancement opens new avenues for advancing photoresponsive supercapacitor technology by leveraging the synergistic effect of photoactivity and electrochemical performance.

3.4 Potential-responsive SCs

Since electrochromic devices undergo reversible color change under the influence of potential, they provide a good opportunity to design potential-responsive smart SCs, which can be used both as color-indicators and energy storage devices. As reported, the performance of potential-responsive smart SCs relies on the electron transfer and the electrolyte ion transfer of electrochromic materials during electrochemical redox reactions. Therefore, the design of nanostructured electrochromic materials with specific structure/morphology, crystal phase

Table 4 Electrochemical performance comparison of photo-responsive SCs

Electrode material	Electrolyte	Potential window (V)	Capacitance (F g^{-1})		Ref.
			Without light illumination	With light illumination	
Thieno[3,2-*b*]thiophene BODIPY	1 M KOH	−0.85–0.1	86 (1 A g^{-1})	134 (1 A g^{-1})	14
FBP_allyl_X electrode	1 M H_2SO_4	0–1.0	190.2 (1 A g^{-1})	369.8 (1 A g^{-1})	97
3D graphene/PEDOT:PSS electrode	PVA/H_3PO_4 electrolyte	0–0.8	534 mF cm^{-3} (3.3 mA cm^{-3})	699.3 mF cm^{-3} (3.3 mA cm^{-3})	98
Vertically aligned ReS_2 nanosheets	1 M KOH	−0.7–0	1.12 mF cm^{-3} (0.375 mA cm^{-2})	21.1 F cm^{-3} (0.375 mA cm^{-2})	30
CoMnS/TiO_2 nanotubes	3 M KOH	0–0.55	42.2 mF cm^{-3} (0.7 mA cm^{-2})	71.7 F cm^{-3} (0.7 mA cm^{-2})	99
Cu_2ZnSnS_4	1 M KCl	−0.1–0.5	41.7 F g^{-1} (5 mV s^{-1})	33.8 F g^{-1} (5 mV s^{-1})	100
WO_3 nanosheets	0.5 M H_2SO_4	−0.5–0	15.3 mF cm^{-3} (0.15 mA cm^{-2})	17.8 F cm^{-3} (0.15 mA cm^{-2})	101
Mn_3O_4/rGO composite	0.5 M KOH	−0.4–0.6	21.9 (0.5 A g^{-1})	13.8 (0.5 A g^{-1})	49
3D nanoporous Cu@Cu_2O array	2 M KOH	0–0.6	567 (1 A g^{-1})	782 (1 A g^{-1})	102
TiO_2/MoO_3 heterojunction	0.5 M H_2SO_4	−0.5–0	38.6 mF cm^{-3} (0.1 mA cm^{-2})	63.2 F cm^{-3} (0.1 mA cm^{-2})	104
CeO_2/MnO_2 heterojunction	1 M Na_2SO_4	0–0.8	187 F g^{-1} (5 mV s^{-1})	229 F g^{-1} (5 mV s^{-1})	105
ZnO/$ZnCo_2O_4$ nanoarrays	PVA-KOH electrolyte	0–0.6	86 μF cm^{-2} (1.2 μA cm^{-2})	150 μF cm^{-2} (1.2 μA cm^{-2})	108

design, high specific area, and high electronic conductivity is beneficial for achieving high-performance smart potential-responsive SCs.

3.4.1 Metal oxide-based materials for potential-responsive SCs. As mentioned before, the electrode materials for potential responsive SCs should possess both electrochromic and energy storage properties. Among these developed electrochromic materials, transition metal oxides (*e.g.*, V_2O_5, WO_3, MnO_2, NiO, and TiO_2),[109–111] which cause color change through bandgap change *via* electrochemical oxidation/reduction reactions, are widely used. Notably, nanomaterials with a large surface area and suitable porosity can improve the electrochromic efficiency by reducing resistance during the charge and mass transport processes. As such, a free-standing V_2O_5 network with a double-gyroid morphology was obtained by electrodeposition into a hollow block copolymer template (Fig. 12a).[112] The transparent electrochromic Li-ion SCs (Fig. 12b), which are assembled using V_2O_5 electrodes with a gyroid-structure grown on a FTO substrate, display a yellow color in the oxidized state while exhibiting a green/gray color in the reduced state (Fig. 12c). Moreover, the obtained Li-ion SCs exhibit a high specific capacitance (155 F g^{-1} at 10 A g^{-1}) and a high energy density of 52 Wh kg^{-1}. Its excellent electrochemical performance is attributed to the V_2O_5 electrode with interconnected porosity, good electronic transport, and large surface area, which reduce the Li^+ ion transport distance and enable the fast lithium-ion insertion/extraction. Owing to the unique color change during the charging/discharging process, the V_2O_5-based electrochromic SCs are promising candidates for the design of smart voltage-responsive SCs.[112]

Apart from symmetric electrochromic SCs, it is also a feasible option to construct electrochromic SCs using suitable asymmetric electrode materials. A full device is assembled by coupling the V_2O_5 nanoflowers/FTO cathode with the WO_{3-x} NWNs/FTO anode (Fig. 12d and e).[113] The device (Fig. 12f) delivers a specific areal capacitance of 18.5 mF cm^{-2} (1 mA cm^{-2}) and maintains a specific areal capacitance of 5.44 mF cm^{-2} (4 mA cm^{-2}), outperforming some of the reported smart electrochromic SCs. It is interesting to note that the color of the device gradually turned dark blue during charging, while it gradually became transparent during discharging, which was attributed to the insertion and extraction of Al^{3+} ions. The results presented here demonstrate the possibility of constructing voltage-responsive smart SCs with dual functions, which not only serve as energy storage devices but also possess electrochromic properties.[113]

As another representative example, a new smart electrochromic SC was constructed by using a WO_3 negative electrode (Fig. 12g) and a MnO_2 positive electrode (Fig. 12h).[114] The obtained device exhibits a color change from pale yellow to dark blue during the charging/discharging process (Fig. 12i), which is due to the combined effect of the color change of the WO_3 negative electrode and the MnO_2 positive electrode (Fig. 12j and k). For the WO_3 negative electrode, the insertion of Li^+ ions causes the reduction of W^{6+} to W^{5+} during the charging process, leading to a color change from transparent to blue, while it returns to its transparent state in the discharging process.

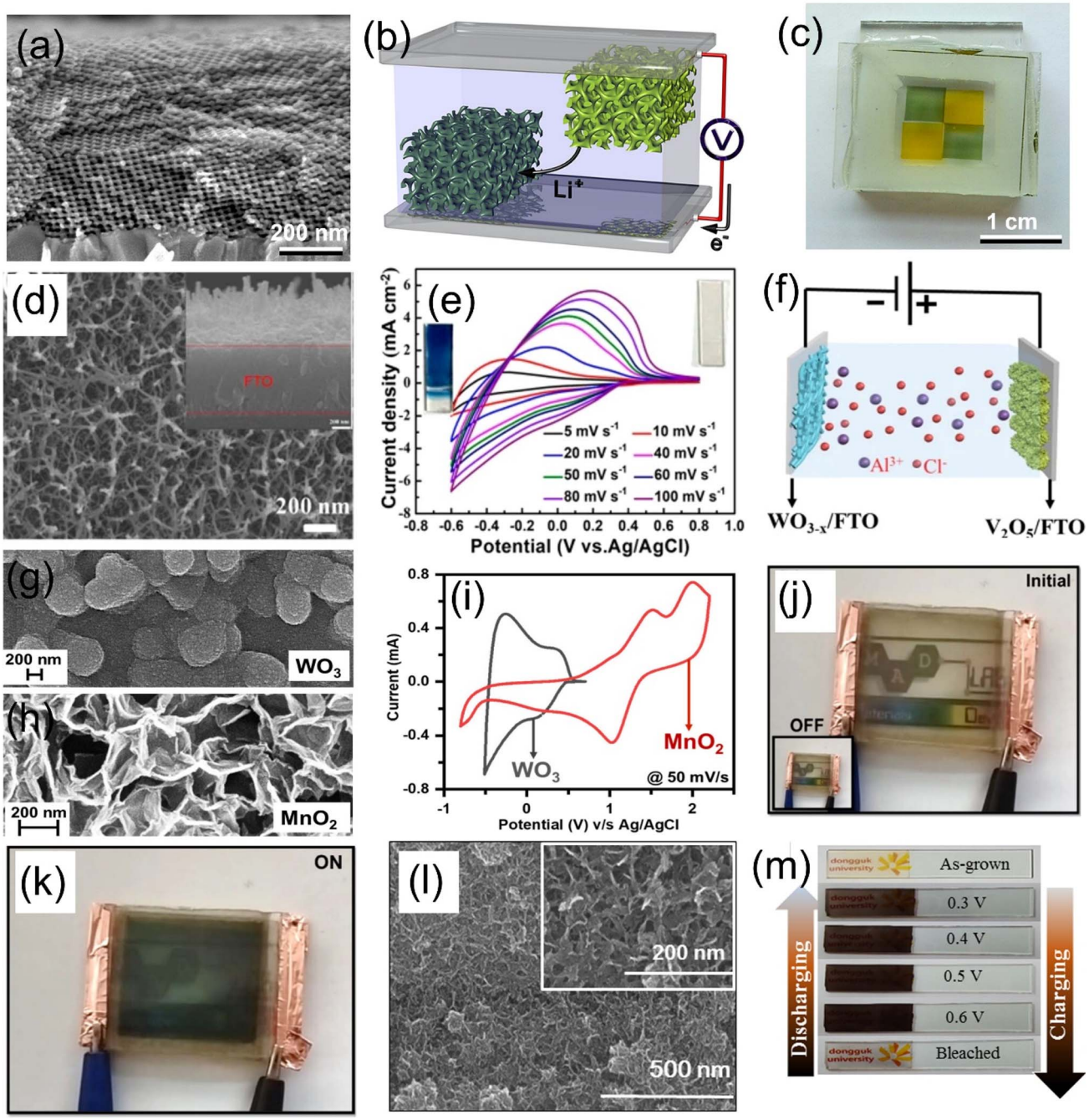

Fig. 12 (a) Cross-sectional SEM image of mesoporous V_2O_5 double-gyroid films. (b) Illustration of the SCs based on V_2O_5 double-gyroid film electrodes. (c) Photograph of transparent electrochromic SCs.[112] Reproduced with permission.[112] Copyright 2012, American Chemical Society. (d) SEM image of the WO_{3-x} NWNs/FTO electrode and its corresponding (e) CV curves at different scan rates. (f) Illustration of the assembly of an electrochromic SC device using the WO_{3-x} NWNs/FTO anode and V_2O_5 nanoflowers/FTO cathode.[113] Reproduced with permission.[113] Copyright 2021, Springer Nature. SEM images of the (g) WO_3 electrode and (h) MnO_2 electrode. (i) CV curves of WO_3 and MnO_2 electrodes at 50 mV s^{-1}. Photographs of the device based on WO_3 and MnO_2 electrodes in (j) initial state and (k) ON state.[114] Reproduced with permission.[114] Copyright 2025, American Chemical Society. (l) SEM images of the $NiMoO_4$ film. (m) Photograph of the $NiMoO_4$ electrode bleached at different voltage potentials.[115] Reproduced with permission.[115] Copyright 2018, Elsevier.

Meanwhile, the color of the MnO_2 electrode changes from pale yellow to dark brown during charging, corresponding to the oxidation of Mn^{3+} to Mn^{4+}, while during discharging, Mn^{4+} is electrochemically reduced to Mn^{3+}, leading to the pale-yellow color of the MnO_2 film due to the detachment of Li^+ ions. Excitingly, the smart electrochromic SC also shows a high specific capacitance (22.6 mF cm^{-2}) and excellent cycle stability. The superior electrochromic properties and the remarkable capacitive behavior suggest its huge potential for use as smart electrochromic SCs.[114]

In addition, bi-metal oxides are also explored to design the voltage-responsive smart electrodes due to the synergistic effects between two different metal elements, thereby leading to enhanced performance in several key areas, such as more efficient charge transport during the coloring and bleaching processes, a wider potential range for redox reactions, and ultrahigh optical modulation across a broader range of the spectrum. As a proof-of-concept, a smart electrochromic SC was built based on a $NiMoO_4$ thin film electrode (Fig. 12l),[115] which was prepared by a simple successive ionic layer adsorption and reaction technique. The nanoflake $NiMoO_4$ film electrode is dark brown in the charged state and becomes transparent in the discharged state (Fig. 12m). Encouragingly, the nanoflake $NiMoO_4$ film electrode exhibits a high specific capacitance of up to 1853 F g^{-1} at 1 A g^{-1} and stable long-cycle performance. The remarkable electrochemical performance and fast and reversible color modulation enable the design the voltage-responsive smart SCs.[115]

3.4.2 Conducting polymer-based materials for potential-responsive SCs. Although inorganic electrochromic materials have shown potential applications in electrochromic SCs, they still suffer from some drawbacks, such as limited color changes and slow switching speeds, thus limiting their large-scale application. Fortunately, organic electrochromic materials, such as organic molecules, polymers, and organic frameworks,[116–118] have attracted tremendous attention as alternative materials for electrochromic SCs because of their rich color selection, fast response rate, and relatively high capacity resulting from multiple redox sites. Representatively, PANI with excellent electrical conductivity is used as an active material for the design of voltage-responsive smart SCs. As an example, a PANI film electrode was synthesized by a combination of galvanostatic and cyclic voltametric electrodeposition techniques (Fig. 13a).[119] The film electrode exhibits multicolor properties with reversible color changes due to three main stable oxidation states of PANI: the fully oxidized pernigraniline

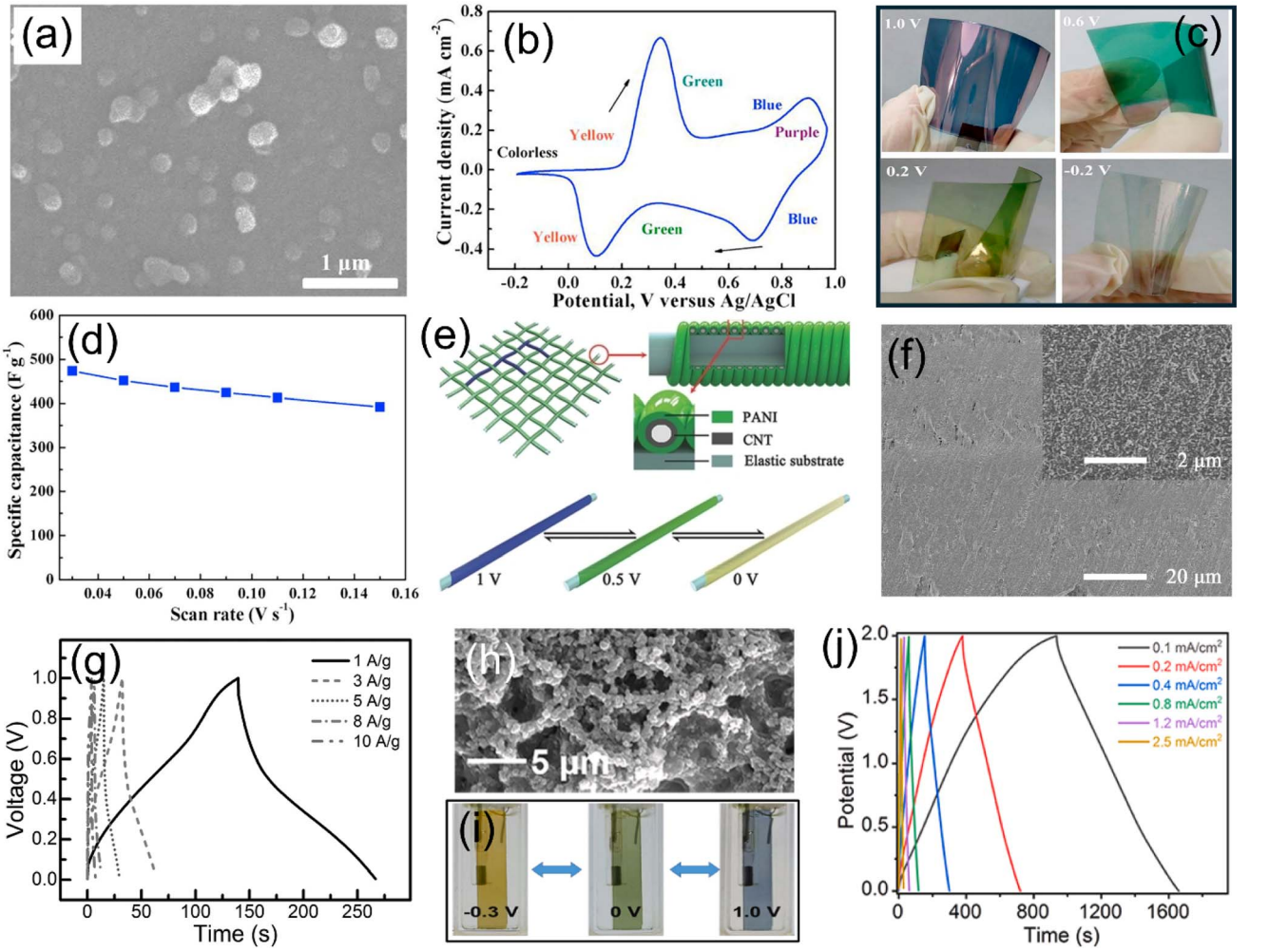

Fig. 13 (a) SEM images of the as-prepared PANI film. (b) CV curve of the as-prepared PANI film electrode. (c) Photograph of the PANI film in color under different potential states. (d) Rate capability of the PANI film electrode.[119] Reproduced with permission.[119] Copyright 2018, Elsevier. (e) Illustration of the structure of the electrochromic SCs based on CNT/PANI fiber. (f) SEM images and (g) charge/discharge curves of the optimized CNT/PANI composite electrode.[120] Reproduced with permission.[120] Copyright 2014, Wiley-VCH. (h) SEM image of the PETOME/ITO electrode and its corresponding (i) photographs under different potential states and (j) charge/discharge curves.[121] Reproduced with permission.[121] Copyright 2023, Elsevier.

form (purple), the 50% oxidized emeraldine form (green), and the fully reduced leucoemeraldine form (transparent yellow). As shown in the CV curve (Fig. 13b), the first oxidation peak (0.34 V) and reduction peak (0.10 V) are attributed to the doping and de-doping of anions, corresponding to the change between leucoemeraldine base and emeraldine salt, while the second oxidation peak (0.9 V) and reduction peak (0.69 V) are associated with the conversion between emeraldine base and pernigraniline base. Furthermore, the color change between these two redox peaks is associated with the conversion of the emeraldine salt and emeraldine base arising from protonation/deprotonation processes (Fig. 13c). Surprisingly, the PANI film electrode delivers a high specific capacitance (473.3 F g^{-1}) at 30 mV s^{-1} and maintains a relatively high capacitance (392.1 F g^{-1}) at 150 mV s^{-1} (Fig. 13d). Its superior electrochemical performance, combined with multiple color states, makes the PANI film electrode a promising candidate for the construction of potential-responsive SCs.[119]

Similarly, an electrochromic fiber-shaped SC was constructed by wrapping an aligned PANI/CNT composite on an elastic fiber (Fig. 13e–g).[120] The obtained SCs exhibit rapid and reversible color changes, which are related to the different oxidation states of PANI. Taking the positive electrode as an example, the relationship between the color change and oxidation state is revealed. When the potential of the PANI/CNTs composite is charged to 1 V, the PANI is in a fully oxidized state, exhibiting a blue color; when the potential is discharged to 0.5 V, the PANI/CNTs composite is in a partially reduced state, showing a green color. Notably, when the electrode is further discharged to −0.5 V or −1 V, the PANI is in a highly reduced state, exhibiting a light yellow color.[120] Additionally, new organic conjugated polymers are attractive

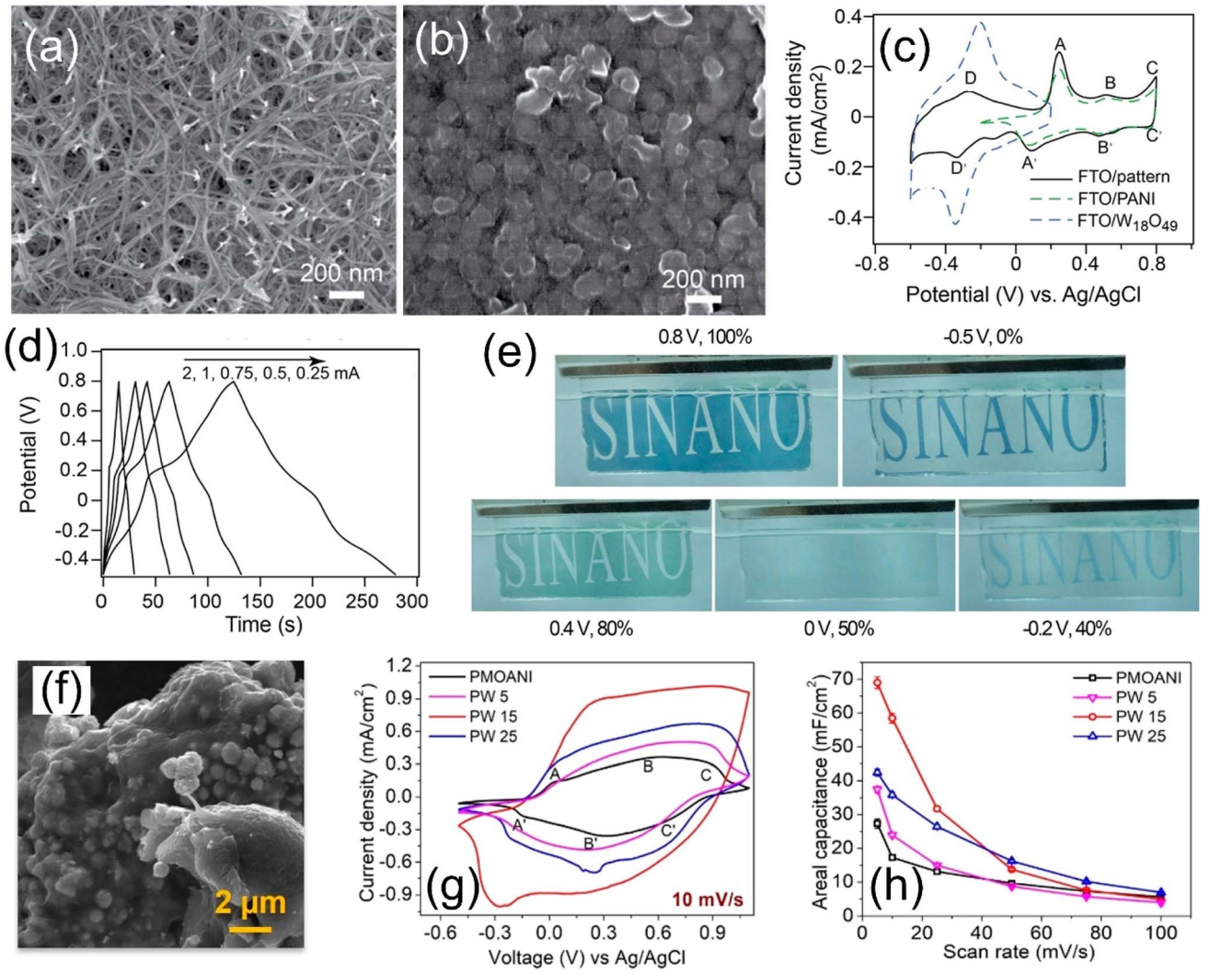

Fig. 14 SEM images of the (a) PANI film and (b) PANI/$W_{18}O_{49}$ composite. (c) CV curves of FTO, PANI, and $W_{18}O_{49}$ electrodes. (d) Charge/discharge curves of the smart SCs based on the PANI/$W_{18}O_{49}$ composite. (e) Photographs of the SC electrodes at several typical states.[122] Reproduced with permission.[122] Copyright 2014, American Chemical Society. (f) SEM image of the PMOANI–WO_3 nanocomposite. (g) CV comparisons of different PMOANI–WO_3 nanocomposites at 10 mV s^{-1}. (h) Areal capacitance of the SCs at different scan rates.[123] Reproduced with permission.[123] Copyright 2023, American Chemical Society.

alternative candidate materials for constructing smart electrochromic SCs. With this in mind, a new conjugated polymer was synthesized *via* a simple electropolymerization method (Fig. 13h).[121] Notably, the color of the PETOME/ITO electrode changes during the electrochromic process: yellow in the anion-doped state (−0.3 V), green in the neutral state (0 V), and finally blue in the cation-doped state (1.0 V) (Fig. 13i), which indicates its multicolor electrochromic behavior due to the integration of EDOT and TPA dual-redox centers.[121] The almost symmetric triangle shape of the charge/discharge curves (Fig. 13j) demonstrates fast electrochemical reaction kinetics and excellent capacitive behavior, which is attributed to the twisted arrangement of the TPA structure, thereby accelerating ion diffusion and reaction kinetics. Encouragingly, coupled with a V_2O_5 nanowire cathode, an asymmetric electrochromic SC was built, which delivers a large potential window (2 V), a high energy density (20.2 μWh cm^{-2}), and a high optical contrast (71.4%). Therefore, it is reasonable to conclude that the rich color change and the remarkable electrochemical performance make the conjugated polymer-based electrode a promising candidate for the design of smart SCs combining energy storage and electrochromic functions.

3.4.3 Composite-based materials for potential-responsive SCs. As reported, transition metal oxides possess some shortcomings, such as long response time and limited color variations. In contrast, conducting polymers have attracted increasing attention due to their rich color variations and relative high capacitance. Nevertheless, conducting polymers suffer from irreversible mechanical degradation and capacity decay because of the repeating doping/de-doping of ions during the redox process. The design of a composite in which a transition metal oxide and a conductive polymer are combined is another effective strategy to build voltage-responsive smart SCs having enhanced properties through synergistic effects.[61] For instance, a smart electrochromic electrode based on the composite of $W_{18}O_{49}$ and PANI was well designed and constructed (Fig. 14a and b).[122] It can be observed that $W_{18}O_{49}$ displays electrochromic behavior in the potential range of −0.5 to 0 V, while PANI shows multicolor behavior in the potential range of 0 to 0.8 V (Fig. 14c). Interestingly, the composite electrode prepared with $W_{18}O_{49}$ and PANI delivers a wide potential range (Fig. 14d), possesses a high specific capacitance and displays various colors (Fig. 14e). By integrating $W_{18}O_{49}$ and PANI into one electrode, the obtained composite electrode not only exhibits excellent capacitive behaviour but also enables new functionality in coloring, thus proving beneficial for the design and construction of high-performance smart electrochromic SCs.[122] Similarly, a facile and low-cost chemical polymerization strategy was employed to prepare a stable and active electrochromic composite material consisting of poly(*o*-methoxyaniline) (PMOANI) and WO_3 nanoflowers (Fig. 14f).[123] The optimized polymer composite not only exhibits pseudocapacitive properties (Fig. 14g) with a large areal capacitance (83 mF cm^{-2}) (Fig. 14h) and good cycle life but also displays color changing characteristics. Amazingly, an asymmetric SC device built using this polymer composite exhibited an areal capacitance of 730 μF cm^{-2} and can switch the color

Table 5 Electrochemical performance comparison of potential-responsive SCs

Electrode material	Electrolyte	Potential window (V)	Capacitance (F g^{-1})	Color change	Ref.
V_2O_5	1 M $LiClO_4$/propylene carbonate solution	2–4	155 (≥10 A g^{-1})	Green/gray/yellow	112
V_2O_5 NFs/FTO	1 M $AlCl_3$	−0.2–0.8	5.64 mF cm^{-2} (5 mV s^{-1})	Light green/transparent	113
WO_{3-x} NWNs/FTO	1 M $AlCl_3$	−0.6–0.8	57.6 mF cm^{-2} (5 mV s^{-1})	Dark blue/transparent	113
WO_3 (anode)	5% PEO + 1 M $LiClO_4$	−0.5–0.7	22.8 mF cm^{-3} (0.1 mA cm^{-2})	Transparent/blue	114
MnO_2 (cathode)	5% PEO + 1 M $LiClO_4$	−0.8–2.2	8.2 mF cm^{-3} (0.1 mA cm^{-2})	Pale yellow/dark brown	114
$NiMoO_4$ thin film	2 M KOH	−0.5–0.7	1853 (1 A g^{-1})	Transparent/dark brown	115
PANI film	0.5 M H_2SO_4	−0.2–1.0	473.3 (30 mV s^{-1})	Transparent/yellow/green/blue/purple	119
PANI/CNTs composite	PVA/H_3PO_4 gel electrolyte	−1.0–1.0	255.5 (1 A g^{-1})	Blue/green/light yellow	120
PETOME/ITO	0.1 M $LiClO_4$	−0.3–1.0	39 mF cm^{-2} (0.1 mA cm^{-2})	Yellow/green/blue	121
$W_{18}O_{49}$/PANI composite	1 M H_2SO_4	−0.5–0.8	24.6 mF cm^{-2}	Transparent/blue	122
PMOANI/WO_3 nanoflowers	1 M $LiClO_4$–PC electrolyte	−1.0–1.0	16.3 mF cm^{-2} (5 mV s^{-1})	Blue/colorless	123
Silver grid/PEDOT:PSS/WO_3 composite	0.5 M H_2SO_4	−0.7–0.1	221.1 (1 A g^{-1})	Blue/transparent	124

between blue and transparent green. The obtained SCs are expected to function as an energy storage device with an additional color indication function, thus making it possible to design potential-based smart SCs.[123]

Subsequently, a silver grid/PEDOT:PSS/WO_3 composite film was fabricated through a unique design.[124] Notably, this film exhibits a noticeable electrochromic properties and a high optical modulation (81.9%), making it highly suitable for electrochromic devices. Using the silver grid/PEDOT:PSS/WO_3 composite as an electrode in an electrochromic SCs, it is observed to exhibit a dark blue color during discharging and a transparent color during charging. The charge and discharge processes are related to the insertion and extraction of H^+ in the WO_3 film. Specifically, the insertion of H^+ leads to the reduction of the W^{6+} ions, thus causing the WO_3 film to appear dark, which corresponds to a decrease in transmittance. During discharging, the extraction of H^+ from the WO_3 film leads to its oxidation back to a higher valence state, which results in a transparent color, accompanied by increased transmittance. The silver grid/PEDOT:PSS/WO_3 hybrid film delivers a specific capacitance of 221.1 F g^{-1} at 1 A g^{-1}, which is larger than those of previously reported WO_3 electrodes. The unique structure and configuration endow the silver grid/PEDOT:PSS/WO_3 hybrid film with high optical modulation and remarkable capacitive behavior, thus making it promising for application in the construction of voltage-responsive smart SCs. According to the above discussion, the construction of nanostructured electrochromic materials with outstanding electron transfer and electrolyte ion transfer capability, unique structure/morphology, and high specific area are beneficial for achieving high-performance smart potential-responsive SCs with multi-functions (Table 5).

4. Future directions and conclusions

Currently, smart stimuli-responsive SCs have attracted increasing attention due to their unique characteristics and multiple functions. Stimuli-responsive SCs are a new generation of energy storage devices whose electrochemical properties can be reversibly and intentionally modulated by applying external triggers like temperature, magnetic field, light, and voltage. These developments could create the next generation of energy storage technology that is not passive but capable of actively interacting with external stimuli, which is crucial for the wearable/portable devices.

The mechanism of smart SCs involves incorporating stimuli-responsive materials (*e.g.*, metal oxides, smart polymers, and photochromic molecules) into electrodes or electrolytes to induce reversible changes in their structure or properties, thereby adjusting or altering their capacitive behavior. Although the research on the primary types of external stimuli (*e.g.*, temperature, magnetic field, light, and voltage) and corresponding stimuli-responsive SCs has made significant progress, there is still a huge room left to further improve the performance of SCs: (a) for thermally responsive supercapacitors, the interfacial contact and electrochemical stability of thermally responsive polymer electrolytes are poor.[125,126] Furthermore, the relatively low ionic conductivity affects the rate performance of SCs. Moreover, further improvements in the switching response rate are needed to shorten the recovery time. Additionally, modifying the electrodes and separator with thermally responsive polymers results in energy density loss due to the weight of additional components; (b) for magnetically responsive SCs, although most research focuses on understanding the effects of magnetic fields on the supercapacitive performance of materials, the origin of magnetic field-dependent supercapacitive properties remains controversial due to the involvement of many interfaces/components. In this context, a thorough investigation of the effects of magnetic fields on all properties of the electrodes and electrolytes is necessary; (c) for photoresponsive SCs, current research mainly focuses on exploring novel electrode materials, while interface design is often overlooked. This is because the performance of photoresponsive electrodes is highly dependent on their morphology, microstructure, and electrode/electrolyte interface. In addition, relatively low areal capacitance, low energy conversion efficiency and the complexity of integrated device design are also major challenges hindering their widespread application;[127] (d) regarding the voltage-responsive SCs, achieving high performance in both electrochromism (color change) and supercapacitance (charge storage) is a challenging task. Typically, improving one property (*e.g.*, coloring efficiency) compromises the other (*e.g.*, specific capacitance). Furthermore, developing electrolytes with a wide operating voltage window, high ionic conductivity, and excellent temperature stability remains a challenge.

Future research in stimuli-responsive SCs is focused on enhancing performance, durability, and multifunctionality for integration into next-generation smart electronics. Some key research directions are shown below: (i) a core direction is the development of novel stimuli-responsive materials (*e.g.*, polymers with dynamic covalent bonding, specific hydrogels, and novel hybrid materials) with tailored properties (*e.g.*, conductivity, porosity, and response times) to push beyond traditional materials; (ii) in addition to the external stimuli mentioned in this review, exploring new stimuli (*e.g.*, mechanical stress and pH) aims to leverage these external factors to overcome the limitations of SCs like low energy density, thus enhancing performance and enabling multifunctional energy storage devices; (iii) future efforts are directed toward understanding the mechanism of the effect of these external stimuli on the resulting SCs, which is critical for the design of high-performance smart SCs. Therefore, more comprehensive studies are needed to reveal the crucial role of each external stimulus in dynamically controlling and optimizing the electrochemical processes, pushing beyond the performance limits of conventional SCs for specialized applications; (iv) this field is still quite new, and there is an urgent need to establish standardized testing procedures and performance benchmarks to ensure comparability between different research products. Moreover, leveraging the latest advances in design guided by theory, simulation, and machine learning will accelerate structural optimization and deepen the understanding of underlying mechanisms. Encapsulation and device-level

integration represent another critical yet often overlooked challenge for the practical deployment of stimuli-responsive SCs. Unlike conventional SCs, these systems rely on dynamic interactions between active materials and external stimuli, which makes them particularly sensitive to environmental factors such as moisture, oxygen, mechanical deformation, and temperature fluctuations. Effective encapsulation must therefore strike a delicate balance between environmental protection and stimuli accessibility. For example, photoresponsive devices require optically transparent yet impermeable barriers, while thermally or mechanically responsive systems demand flexible and thermally conductive packaging materials that do not hinder their response behavior.[128] In addition, maintaining the long-term stability of electrolyte systems (*e.g.*, hydrogels or polymer-based electrolytes) under encapsulated conditions remains a major challenge due to potential dehydration, leakage, or chemical degradation.[129,130] The integration of encapsulation layers can also introduce additional interfacial resistance and increase device weight, thereby compromising electrochemical performance.[131] Consequently, the development of advanced encapsulation strategies, such as multifunctional barrier materials, self-healing coatings, and flexible thin-film packaging, will be essential to ensure durability, reliability, and real-world applicability of smart stimuli-responsive SCs.[132]

In summary, this paper briefly reviews the latest research progress in the design of stimulus-responsive SCs, focusing primarily on the synthesis of stimulus-responsive electrodes and their response characteristics/functions. Furthermore, it discusses the role of various external forces/stimuli in enhancing capacitance performance, particularly their interactions with the components of SCs. Finally, this paper also outlines the challenges and future research directions in this field. In a word, this paper not only provides a reference for the design and construction of smart responsive SCs but also offers valuable information for other researchers in this field.

Conflicts of interest

There are no conflicts of interest to declare.

Data availability

Data availability does not apply to this review paper as no new data are generated or analysed as part of this review.

Acknowledgements

The authors would like to acknowledge the funding support from the Nanyang Technological University Startup Grant, the Singapore Ministry of Education Academic Research Fund Tier1 Grant (RS30/23), the University of Waterloo and the Natural Science and Engineering Research Council of Canada.

References

1 J. He, L. Cao, J. Cui, G. Fu, R. Jiang, X. Xu and C. Guan, *Adv. Mater.*, 2024, **36**, 2306090.
2 M. Yu, Y. Peng, X. Wang and F. Ran, *Adv. Funct. Mater.*, 2023, **33**, 2301877.
3 P. Zhang, F. Zhu, F. Wang, J. Wang, R. Dong, X. Zhuang, O. G. Schmidt and X. Feng, *Adv. Mater.*, 2017, **29**, 1604491.
4 U. Jeong and Y. Yin, *Adv. Funct. Mater.*, 2020, **30**, 1907059.
5 H. Parsimehr and A. Ehsani, *Chem. Rec.*, 2022, **22**, e202200075.
6 P. Pandey, P. Ray, A. Sharma and M. Qureshi, *Appl. Phys. Lett.*, 2024, **124**, 140503.
7 J. Zhuang, M. R. Gordon, J. Ventura, L. Li and S. Thayumanavan, *Chem. Soc. Rev.*, 2013, **42**, 7421–7435.
8 C. Li, K. Wang, J. Li and Q. Zhang, *ACS Mater. Lett.*, 2020, **2**, 779–797.
9 Y. Zhou, H. Qi, J. Yang, Z. Bo, F. Huang, M. S. Islam, X. Lu, L. Dai, R. Amal, C. H. Wang and Z. Han, *Energy Environ. Sci.*, 2021, **14**, 1854–1896.
10 R. Wang, M. Yao and Z. Niu, *InfoMat*, 2020, **2**, 113–125.
11 J. C. Kelly, M. Pepin, D. L. Huber, B. C. Bunker and M. E. Roberts, *Adv. Mater.*, 2012, **24**, 886–889.
12 J. C. Kelly, R. Gupta and M. E. Roberts, *J. Mater. Chem. A*, 2015, **3**, 4026–4034.
13 V. Sharma, S. Biswas and A. Chandra, *Adv. Energy Mater.*, 2018, **8**, 1800573.
14 M. Özdemir, S. Uluçay, E. Sevimli, S. Altınışık, B. Köksoy, B. Yalçın and S. Koyuncu, *ACS Appl. Energy Mater.*, 2025, **8**, 17232–17245.
15 J. Muñoz, *Adv. Mater.*, 2024, **36**, 2305546.
16 V. Kumar, S. Park, K. Parida, V. Bhavanasi and P. S. Lee, *Mater. Today Energy*, 2017, **4**, 41–57.
17 S. Guragain, B. P. Bastakoti, V. Malgras, K. Nakashima and Y. Yamauchi, *Chem.–Eur. J.*, 2015, **21**, 13164–13174.
18 H. Zhang, W. Li, Q. Huang, G. Huang, Z. Chi and B. S. Li, *Dyes Pigm.*, 2021, **187**, 109128.
19 R. Zheng, Y. Wei, Z.-C. Zhang, Z.-Y. Wang, L.-L. Ma, Y. Wang, L. Huang and Y.-Q. Lu, *Responsive Mater.*, 2023, **1**, e20230017.
20 M. Deepa, R. Sharma, A. Basu and S. A. Agnihotry, *Electrochim. Acta*, 2005, **50**, 3545–3555.
21 W. Wu, S. Guo, J. Bian, X. He, H. Li and J. Li, *J. Energy Chem.*, 2024, **93**, 453–470.
22 H. Zhang, P. Xue, J. Liu and X. Xu, *ACS Appl. Energy Mater.*, 2021, **4**, 6116–6124.
23 V. H. Nguyen, R. Tabassian, S. Oh, S. Nam, M. Mahato, P. Thangasamy, A. Rajabi-Abhari, W.-J. Hwang, A. K. Taseer and I.-K. Oh, *Adv. Funct. Mater.*, 2020, **30**, 1909504.
24 D. Zhang, B. Ren, Y. Zhang, L. Xu, Q. Huang, Y. He, X. Li, J. Wu, J. Yang, Q. Chen, Y. Chang and J. Zheng, *J. Mater. Chem. B*, 2020, **8**, 3171–3191.
25 J. Wei, C. Ma, T. Zhang, Z. Shao and Y. Chen, *Chem. Eng. J.*, 2024, **490**, 151393.
26 H. Yang, Z. Liu, B. K. Chandran, J. Deng, J. Yu, D. Qi, W. Li, Y. Tang, C. Zhang and X. Chen, *Adv. Mater.*, 2015, **27**, 5593–5598.
27 Y. Dou, T. Pan, A. Zhou, S. Xu, X. Liu, J. Han, M. Wei, D. G. Evans and X. Duan, *Chem. Commun.*, 2013, **49**, 8462–8464.

28 Y. Shi, H. Ha, A. Al-Sudani, C. J. Ellison and G. Yu, *Adv. Mater.*, 2016, **28**, 7921–7928.
29 J. Zhu, M. Chen, H. Wei, N. Yerra, N. Haldolaarachchige, Z. Luo, D. P. Young, T. C. Ho, S. Wei and Z. Guo, *Nano Energy*, 2014, **6**, 180–192.
30 N. Arya, P. Avasthi and V. Balakrishnan, *Nanoscale Adv.*, 2021, **3**, 2089–2102.
31 Y.-J. Kim and Y. T. Matsunaga, *J. Mater. Chem. B*, 2017, **5**, 4307–4321.
32 D. Roy, W. L. A. Brooks and B. S. Sumerlin, *Chem. Soc. Rev.*, 2013, **42**, 7214–7243.
33 K. Ryu, G. Li, K. Zhang, J. Guan, Y. Long and Z. Dong, *Acc. Mater. Res.*, 2025, **6**, 379–392.
34 B. Wang, W. Liang, Z. Guo and W. Liu, *Chem. Soc. Rev.*, 2015, **44**, 336–361.
35 Y. Zhu, R. Batchelor, A. B. Lowe and P. J. Roth, *Macromol.*, 2016, **49**, 672–680.
36 Y. Hiruta, *Polym. J.*, 2022, **54**, 1419–1430.
37 T. Yu, P. Xue, S. Ma, Y. Gu, Y. Wang and X. Xu, *ChemistrySelect*, 2022, **7**, e202104499.
38 H. Jiang, R. K. Emmett and M. E. Roberts, *J. Appl. Electrochem.*, 2019, **49**, 271–280.
39 P. Zhang, J. Wang, W. Sheng, F. Wang, J. Zhang, F. Zhu, X. Zhuang, R. Jordan, O. G. Schmidt and X. Feng, *Energy Environ. Sci.*, 2018, **11**, 1717–1722.
40 Y. Yang, D. Yu, H. Wang and L. Guo, *Adv. Mater.*, 2017, **29**, 1703040.
41 J. Zhu, M. Yao, S. Huang, J. Tian and Z. Niu, *Angew. Chem., Int. Ed.*, 2020, **59**, 16480–16484.
42 Y. Shi, Q. Zhang, Y. Zhang, L. Jia and X. Xu, *ACS Appl. Mater. Interfaces*, 2018, **10**, 7171–7179.
43 S. Ma, Y. Shi, Y. Zhang, L. Zheng, Q. Zhang and X. Xu, *ACS Appl. Mater. Interfaces*, 2019, **11**, 29960–29969.
44 M. Li and Z. Chen, *J. Polym. Sci.*, 2021, **59**, 2230–2245.
45 Z. Chen, P.-C. Hsu, J. Lopez, Y. Li, J. W. F. To, N. Liu, C. Wang, S. C. Andrews, J. Liu, Y. Cui and Z. Bao, *Nat. Energy*, 2016, **1**, 15009.
46 L. Zhang, Z. Zeng, D.-W. Wang, Y. Zuo, J. Chen and X. Yan, *Cell Rep. Phys. Sci.*, 2021, **2**, 100455.
47 S. Raj K A and C. S. Rout, *J. Mater. Chem. A*, 2023, **11**, 5495–5519.
48 K. M. Grant, J. W. Hemmert and H. S. White, *Electrochem. Commun.*, 1999, **1**, 319–323.
49 A. Joby, P. Kumbhakar and M. Balachandran, *Emergent Mater.*, 2024, **7**, 2393–2406.
50 R. N. O'Brien and K. S. V. Santhanam, *J. Appl. Electrochem.*, 1997, **27**, 573–578.
51 G. Hinds, J. M. D. Coey and M. E. G. Lyons, *Electrochem. Commun.*, 2001, **3**, 215–218.
52 N. Leventis and X. Gao, *J. Am. Chem. Soc.*, 2002, **124**, 1079–1088.
53 S. Mohanta and T. Z. Fahidy, *J. Appl. Electrochem.*, 1978, **8**, 265–267.
54 C. M. Costa, K. J. Merazzo, R. Gonçalves, C. Amos and S. Lanceros-Méndez, *iScience*, 2021, **24**, 102691.
55 G. Hinds, F. E. Spada, J. M. D. Coey, T. R. Ní Mhíocháin and M. E. G. Lyons, *J. Phys. Chem. B*, 2001, **105**, 9487–9502.
56 P. Personnettaz, S. Landgraf, M. Nimtz, N. Weber and T. Weier, *Electrochem. Commun.*, 2019, **105**, 106496.
57 M. Waskaas and Y. I. Kharkats, *J. Phys. Chem. B*, 1999, **103**, 4876–4883.
58 S. C. Lau, H. N. Lim, T. B. S. A. Ravoof, M. H. Yaacob, D. M. Grant, R. C. I. MacKenzie, I. Harrison and N. M. Huang, *Electrochim. Acta*, 2017, **238**, 178–184.
59 R. Zhou, Y. Peng, X. Yang, Y. Yang, X. Li, Y. Gao, L. Wang and W. Lü, *J. Alloys Compd.*, 2025, **1021**, 179587.
60 A. Bibi, M. Mustaqeem, M. A. Gondal, A. Majeed, P.-T. Chou, Y.-F. Chen, Z.-G. Gu, M. Waqas and A. Ali, *J. Energy Storage*, 2025, **123**, 116696.
61 M. Rakibuddin and H. Kim, *New J. Chem.*, 2017, **41**, 15327–15333.
62 A. Sood, A. D. Poletayev, D. A. Cogswell, P. M. Csernica, J. T. Mefford, D. Fraggedakis, M. F. Toney, A. M. Lindenberg, M. Z. Bazant and W. C. Chueh, *Nat. Rev. Mater.*, 2021, **6**, 847–867.
63 J. Li, Y. Zhuang, J. Chen, B. Li, L. Wang, S. Liu and Q. Zhao, *EnergyChem*, 2021, **3**, 100060.
64 W. Zhang, H. Li, E. Hopmann and A. Y. Elezzabi, *Nanophotonics*, 2021, **10**, 825–850.
65 M. Deepa, D. P. Singh, S. M. Shivaprasad and S. A. Agnihotry, *Curr. Appl. Phys.*, 2007, **7**, 220–229.
66 W. Kang, C. Yan, X. Wang, C. Y. Foo, A. W. Ming Tan, K. J. Zhi Chee and P. S. Lee, *J. Mater. Chem. C*, 2014, **2**, 4727–4732.
67 C. D. Wessells, R. A. Huggins and Y. Cui, *Nat. Commun.*, 2011, **2**, 550.
68 C. D. Wessells, S. V. Peddada, M. T. McDowell, R. A. Huggins and Y. Cui, *J. Electrochem. Soc.*, 2011, **159**, A98.
69 M. Qiu, F. Zhou, P. Sun, X. Chen, C. Zhao and W. Mai, *Nano Energy*, 2020, **78**, 105148.
70 X. Wang, L. Guo, S. Cao and W. Zhao, *Chem. Phys. Lett.*, 2020, **749**, 137434.
71 L. Striepe and T. Baumgartner, *Chem.–Eur. J.*, 2017, **23**, 16924–16940.
72 S. Zhang, S. Chen, Y. Cao, F. Yang, H. Peng, B. Yan, H. Jiang, Y. Gu and M. Xiang, *J. Mater. Sci.: Mater. Electron.*, 2019, **30**, 13497–13508.
73 M. Tao, G. Liu, Y. Wang, J. Wang, W. Zhang and Z. Li, *ACS Appl. Mater. Interfaces*, 2024, **16**, 54316–54327.
74 M. Marzocchi, I. Gualandi, M. Calienni, I. Zironi, E. Scavetta, G. Castellani and B. Fraboni, *ACS Appl. Mater. Interfaces*, 2015, **7**, 17993–18003.
75 Z. Liu, H. I. Wang, A. Narita, Q. Chen, Z. Mics, D. Turchinovich, M. Kläui, M. Bonn and K. Müllen, *J. Am. Chem. Soc.*, 2017, **139**, 9443–9446.
76 A. Teixeira do Nascimento, P. R. Stoddart, T. Goris, M. Kael, R. Manasseh, K. Alt, J. Tashkandi, B. C. Kim and S. E. Moulton, *Adv. Mater.*, 2025, **37**, e07559.
77 S. Chen, Y. Li, Y. Feng and W. Feng, *Mater. Chem. Front.*, 2023, **7**, 1562–1590.
78 P. Yang, C. Feng, Y. Liu, T. Cheng, X. Yang, H. Liu, K. Liu and H. J. Fan, *Adv. Energy Mater.*, 2020, **10**, 2002898.

79 S. Tan, Z. Zhang, Y. Xue, J. Zhao, J. Ji, C. Wang and Y. Wu, *Ind. Eng. Chem. Res.*, 2023, **62**, 2741–2751.
80 S. Liu, S. Ma, Q. Zhang and X. Xu, *Ionics*, 2022, **28**, 5119–5128.
81 F. Mo, H. Li, Z. Pei, G. Liang, L. Ma, Q. Yang, D. Wang, Y. Huang and C. Zhi, *Sci. Bull.*, 2018, **63**, 1077–1086.
82 Q. Wang and L. Zhang, *ACS Nano*, 2021, **15**, 149–174.
83 M. Singh, A. Sahoo, K. L. Yadav and Y. Sharma, *ACS Appl. Mater. Interfaces*, 2020, **12**, 49530–49540.
84 P. Haldar, S. Biswas, V. Sharma and A. Chandra, *J. Electrochem. Soc.*, 2018, **165**, A3230.
85 A. González, E. Goikolea, J. A. Barrena and R. Mysyk, *Renewable Sustainable Energy Rev.*, 2016, **58**, 1189–1206.
86 J. Bhagwan, A. Sahoo, K. L. Yadav and Y. Sharma, *Electrochim. Acta*, 2015, **174**, 992–1001.
87 M. Singh, B. P. Dubey, A. Sahoo, K. L. Yadav and Y. Sharma, *J. Energy Storage*, 2021, **44**, 103361.
88 W. Tian, P. Ren, X. Hou, R. Xue, Z. Chen, Z. Guo, Y. Jin and F. Ren, *Int. J. Biol. Macromol.*, 2024, **261**, 129977.
89 H. Wei, H. Gu, J. Guo, D. Cui, X. Yan, J. Liu, D. Cao, X. Wang, S. Wei and Z. Guo, *Adv. Compos. Hybrid Mater.*, 2018, **1**, 127–134.
90 S. Pal, S. Majumder, S. Dutta, S. Banerjee, B. Satpati and S. De, *J. Phys. D: Appl. Phys.*, 2018, **51**, 375501.
91 J. Zhu, M. Chen, H. Qu, Z. Luo, S. Wu, H. A. Colorado, S. Wei and Z. Guo, *Energy Environ. Sci.*, 2013, **6**, 194–204.
92 Z. Zeng, Y. Liu, W. Zhang, H. Chevva and J. Wei, *J. Power Sources*, 2017, **358**, 22–28.
93 G. Wang, H. Xu, L. Lu and H. Zhao, *J. Energy Chem.*, 2014, **23**, 809–815.
94 M. C. Fite, J.-Y. Rao and T. Imae, *Bull. Chem. Soc. Jpn.*, 2020, **93**, 1139–1149.
95 Y. Zhao, H. Li, R. Tang, X. Wang, Y. Wu, S. Yan and Y. Zhang, *J. Mater. Chem. A*, 2023, **11**, 15844–15854.
96 J. Zhao, K. Xu, W. Yang, Z. Wang and F. Zhong, *Chem. Soc. Rev.*, 2015, **44**, 8904–8939.
97 S. Altınışık, *ACS Omega*, 2026, **11**, 1826–1853.
98 F. Yi, H. Ren, K. Dai, X. Wang, Y. Han, K. Wang, K. Li, B. Guan, J. Wang, M. Tang, J. Shan, H. Yang, M. Zheng, Z. You, D. Wei and Z. Liu, *Energy Environ. Sci.*, 2018, **11**, 2016–2024.
99 M. M. Momeni, M. Najafi, H. Farrokhpour and B.-K. Lee, *J. Energy Storage*, 2024, **79**, 109666.
100 S. P. Madhusudanan, M. Suresh Kumar, K. Yamini Yasoda, D. Santhanagopalan and S. K. Batabyal, *J. Mater. Sci.: Mater. Electron.*, 2020, **31**, 752–761.
101 M. Zhu, Y. Huang, Y. Huang, Z. Pei, Q. Xue, H. Li, H. Geng and C. Zhi, *Adv. Funct. Mater.*, 2016, **26**, 4481–4490.
102 C. An, Z. Wang, W. Xi, K. Wang, X. Liu and Y. Ding, *J. Mater. Chem. A*, 2019, **7**, 15691–15697.
103 T. Fang, H. Hu, J. Liu, M. Jiang, S. Zhou, J. Fu, W. Wang and Y. Yang, *J. Phys. Chem. C*, 2021, **125**, 18734–18742.
104 B. Ezhilmaran, S. Madhavanunni Rekha and S. Venkataprasad Bhat, *Batteries Supercaps*, 2025, **8**, e202400654.
105 W. Yang, J. Wang, S. Gao, H. Zhang, H. Wang and Q. Li, *J. Adv. Ceram.*, 2022, **11**, 1735–1750.
106 C. Yuan, H. Yin, H. Lv, Y. Zhang, J. Li, D. Xiao, X. Yang, Y. Zhang and P. Zhang, *JACS Au*, 2023, **3**, 3127–3140.
107 Y. Wang, H. Fang, S. Liang, X. Sheng, Y. Huang, Y. Zhang and Y. Zhou, *Appl. Surf. Sci.*, 2022, **606**, 154872.
108 B. D. Boruah and A. Misra, *ACS Appl. Energy Mater.*, 2019, **2**, 278–286.
109 T. Rao, Y. Zhou, J. Jiang, P. Yang and W. Liao, *Nano Energy*, 2022, **100**, 107479.
110 S. Kandpal, T. Ghosh, C. Rani, A. Chaudhary, J. Park, P. S. Lee and R. Kumar, *ACS Energy Lett.*, 2023, **8**, 1870–1886.
111 Y. Huang, B. Wang, F. Chen, Y. Han, W. Zhang, X. Wu, R. Li, Q. Jiang, X. Jia and R. Zhang, *Adv. Opt. Mater.*, 2022, **10**, 2101783.
112 D. Wei, M. R. J. Scherer, C. Bower, P. Andrew, T. Ryhänen and U. Steiner, *Nano Lett.*, 2012, **12**, 1857–1862.
113 S. Wang, H. Xu, T. Hao, P. Wang, X. Zhang, H. Zhang, J. Xue, J. Zhao and Y. Li, *NPG Asia Mater.*, 2021, **13**, 51.
114 N. Ahlawat, L. Bansal, B. Sahu, D. K. Rath, S. Tiwari, A. Chaudhary, S. Kaladi Chondath and R. Kumar, *ACS Appl. Energy Mater.*, 2025, **8**, 4288–4298.
115 H. S. Chavan, B. Hou, A. T. A. Ahmed, Y. Jo, S. Cho, J. Kim, S. M. Pawar, S. Cha, A. I. Inamdar, H. Im and H. Kim, *Sol. Energy Mater. Sol. Cells*, 2018, **185**, 166–173.
116 Y. Wang, S. Wang, X. Wang, W. Zhang, W. Zheng, Y.-M. Zhang and S. X.-A. Zhang, *Nat. Mater.*, 2019, **18**, 1335–1342.
117 P. Shi, C. M. Amb, E. P. Knott, E. J. Thompson, D. Y. Liu, J. Mei, A. L. Dyer and J. R. Reynolds, *Adv. Mater.*, 2010, **22**, 4949–4953.
118 S. Xiong, Y. Wang, X. Wang, J. Chu, R. Zhang, M. Gong, B. Wu and Z. Li, *Sol. Energy Mater. Sol. Cells*, 2020, **209**, 110438.
119 K. Zhou, H. Wang, J. Jiu, J. Liu, H. Yan and K. Suganuma, *Chem. Eng. J.*, 2018, **345**, 290–299.
120 X. Chen, H. Lin, J. Deng, Y. Zhang, X. Sun, P. Chen, X. Fang, Z. Zhang, G. Guan and H. Peng, *Adv. Mater.*, 2014, **26**, 8126–8132.
121 Y. Xie, Y. Zhang, M. Zhu, R. Huang and D. Chao, *Dyes Pigm.*, 2023, **208**, 110889.
122 Y. Tian, S. Cong, W. Su, H. Chen, Q. Li, F. Geng and Z. Zhao, *Nano Lett.*, 2014, **14**, 2150–2156.
123 P. Dutta, S. C. Karumuthil, R. Roy and A. K. Singh, *ACS Appl. Polym. Mater.*, 2023, **5**, 4088–4099.
124 G. Cai, P. Darmawan, M. Cui, J. Wang, J. Chen, S. Magdassi and P. S. Lee, *Adv. Energy Mater.*, 2016, **6**, 1501882.
125 X. Song, X. Dong, H. Liu, Z. Wang and Q. Cao, *ChemSusChem*, 2026, **19**, e202501440.
126 C.-Y. Hsu, F. Alnaimat, G. PadmaPriya, S. Al-Hasnaawei, M. Najafloo, M. Dehghanipour, S. Ray, K. Chennakesavulu, R. Sharma and A. S. Chauhan, *Mater. Today Chem.*, 2026, **51**, 103338.
127 Y. Kim, H. Bark, A. Gupta, Y. Zhang, J. lee and P. S. Lee, *Adv. Energy Mater.*, 2025, **15**, 2405480.
128 J. Kim, M. S. Kim and H. J. Kim, *Adv. Energy Mater.*, 2018, **8**, 1702028.

129 X. Wang, B. Liu and Q. Wang, *Chem. Soc. Rev.*, 2019, **48**, 162–191.
130 C. Yang and Z. Suo, *Nat. Rev. Mater.*, 2018, **3**, 125–142.
131 L. Hu, H. Wu and Y. Cui, *Energy Environ. Sci.*, 2011, **4**, 642–646.
132 D.-H. Kim, N. Lu, R. Ma and J. A. Rogers, *Science*, 2011, **333**, 838–843.